Organic fouling control through magnetic ion exchangeânanofiltration (MIEXâNF) in water treatment

Organic Fouling Control through Magnetic Ion Exchange-Nanofiltration (MIEX-NF) in Water Treatment

Alessandra Imbrogno[a]*, Alberto Tiraferri[b], Sara Abbenante[a,b], Stephan Weyand[c], Ruth Schwaiger[c,d], Thomas Luxbacher[e], Andrea I. Schäfer[a]

[a] Membrane Technology Department, Institute of Functional Interfaces, Karlsruhe Institute of Technology (KIT), Hermann-von-Helmholtz-Platz 1, 76344 Eggenstein-Leopoldshafen, Germany

[b] Department of Environment, Land and Infrastructure Engineering (DIATI), Politecnico di Torino, Turin, Italy, Corso Duca degli Abruzzi 24, 10129, Turin, Italy

[c] Institute for Applied Materials, Karlsruhe Institute of Technology (KIT), Hermann-von-Helmholtz-Platz 1, 76344 Eggenstein-Leopoldshafen, Germany

[d] Karlsruhe Nano Micro Facility (KNMF), Karlsruhe Institute of Technology (KIT), Hermann-von-Helmholtz-Platz 1, 76344 Eggenstein-Leopoldshafen, Germany

[e] Anton Paar GmbH, Anton-Paar-Str. 20, 8054 Graz, Austria

*Corresponding author

alessandra.imbrogno@kit.edu

phone number: +49 (0)721 608 2 8229

Abstract

Magnetic ion exchange resins (MIEX) were combined with nanofiltration (NF) in one single process to mitigate fouling by humic acids (HA). MIEX effectiveness in controlling NF fouling was investigated under different feed chemical conditions and employing two types of NF membranes (NF270, NF90). Fouling layer thickness was determined using novel helium ion microscopy, which allowed analysis of the membrane surface without sample alteration. Without MIEX, significant flux reduction (53-78%) due to irreversible organic fouling was observed for NF90, while fouling of NF270 membranes was mostly reversible (15-23% irreversible flux reduction). This difference stems partially from the different ability of the two membranes to reject calcium, which affects the deposition of HA. Fouling was generally higher at alkaline pH due to calcite precipitation and formation of calcium-HA complexes. In the combined MIEX-NF process, fouling was reduced significantly. With NF90, irreversible flux reduction was half compared to the experiments run without resins, especially at neutral and alkaline pH (6-10). This was attributed to favorable HA-MIEX electrostatic interaction, which minimized the Ca-HA complexation and the availability of foulants for membrane deposition. Results demonstrated the effectiveness of MIEX to minimize fouling under different feed chemical conditions. This is of great importance considering the wide variability of real water chemistries in NF sources for drinking water production.

Keywords

Nanofiltration, Fouling, Helium-Ion-Microscopy, Magnetic ion exchange (MIEX®), Humic acid

1. Introduction

Application of nanofiltration (NF) in drinking water applications is constantly growing as this membrane process can separate divalent salts and small organic molecules to produce high quality water [1-3]. Natural organic matter (NOM) is one of the most common contaminants present in all water resources. Removing NOM is important because of its undesirable odor, taste and color, and because it is responsible for bacterial re-growth and reaction with chlorine disinfectants to produce disinfection-by-products (DBPs) [4, 5]. Long-term adverse health effects of DBPs are widely reported in the literature and the amount of these substances in drinking water is regulated strictly [6-8].

A large fraction of NOM, e.g. polysaccharides and humic acids (HA), is highly retained by NF/RO membranes mostly due to size exclusion, charge repulsion, and hydrophobic interactions [9-11]. Further, NOM is the main culprit of membrane organic fouling, which reduces system performance as a consequence of the deposition of suspended and dissolved organic substances onto the membrane surface and within its pores [12]. Fouling is associated with reduced productivity and deterioration of product water quality, increased energy demand and maintenance costs, membrane degradation, and reduced membrane life [13]. Indeed, fouling is a great challenge that engineers struggle to overcome for the full implementation of membrane technology in drinking water production, especially when treating water sources containing high concentrations of NOM and other organic substances [14, 15].

The main factors influencing membrane fouling by NOM are: i) the surface structure and the chemical properties of the membrane [16-19], ii) the chemical composition of the feed solution [13, 20-22] and iii) the operating conditions [20-24]. Several studies have reported an increase in fouling in the presence of divalent cations, especially calcium, due to the related reduction of organic dissolution rate [25] and to bridging interactions of NOM functional groups (mainly COOH and OH) with those of the membrane surface [21, 26-30]. This effect is more pronounced under alkaline pH conditions, as ionization of carboxyl groups promotes complexation with calcium cations [31] and the solubility of calcium is lower [27]. Wang *et al.* [31] observed that Ca-HA complexes are highly sensitive to pH changes and to calcium concentration; they suggested the existence of a critical foulant size of roughly 300-400 nm. Mo *et al.* [32] demonstrated that the density of available surface carboxyls at the membrane-solution interface plays a key role in promoting fouling by NOM. Specifically, lower flux decline, greater fouling reversibility

and cleaning efficiency were observed when the carboxyl group density was lower. However, at acidic pH and especially at high ionic strength, the electrostatic repulsion between the membrane and NOM molecules is reduced, resulting in more favorable organic deposition on the membrane surface [10, 26].

While important progress has been achieved to understand fouling mechanisms and to develop anti-fouling membranes, organic fouling remains of critical concern in NF. New strategies are required for fouling mitigation as well as for optimization of pre-treatment. Feed pre-treatment (including coagulation, activated carbon, ozonation, H_2O_2/UV oxidation, and ion exchange) modifies NOM characteristics with the goal to reduce its interactions with the membrane [13]. Advanced oxidation processes modify the functional groups and the structure of NOM to yield less hydrophobic and sorbable compounds [33, 34]. Coagulants (e.g., iron or aluminum salts) and granular activated carbon remove high molecular weight and hydrophobic organic compounds, respectively, resulting in reduced membrane fouling [35-38]. Ion exchange resins have been applied successfully in feed pre-treatment due to their high NOM removal capacity [39-41]. Magnetic ion exchange resins (MIEX) were developed specifically for the removal of NOM in drinking water treatment [42-45]. These resins are advantageous compared with conventional ion exchange resins due to: i) their smaller size, ii) easy downstream recovery made possible by their magnetic properties, and iii) higher kinetics of NOM adsorption and surface regeneration due to the larger specific area and more active exchange sites [46, 47].

MIEX resins have been used in combination with biological activated carbon to pre-treat secondary wastewater effluents, thus reducing NF membrane fouling [48, 49]. Son *et al.* [50] investigated MIEX application to mitigate fouling of UF membranes. The removal efficiency of MIEX was shown to be higher for the low molecular weight organic fraction (< 10 kDa). This is of great importance for pre-treatment in NF process where convective transport of the low molecular fraction of NOM occurs at high recovery rates [9]. MIEX packed in fluidized bed column was combined with submerged NF membranes [39]. MIEX significantly removed NOM compounds characterized by low specific ultraviolet absorbance (SUVA) values (mainly phenolic compounds, aliphatic hydrocarbon, and amino sugars). Lower removal efficiency was determined for carboxyl-containing substances. Flux decline in the subsequent NF step was reduced by 30% and MIEX use also resulted in reduced biofouling, suggesting MIEX as an effective pre-treatment for NF.

In the present study, MIEX and NF are combined in one single process to investigate and mitigate fouling by HA. Previously, MIEX was used mostly in feed pre-treatment, while no studies about direct application in the membrane system has been reported. Further, compared with fluidized bed columns, stirred reactors increase turbulence, thus decreasing the resistance to liquid phase mass transfer and leading to better interaction of MIEX and HA. Initially, static adsorption studies of HA by MIEX are

discussed to elucidate MIEX-HA interactions. MIEX effectiveness in controlling NF fouling is thus investigated. Two types of widely employed commercial NF membranes (a loose and a tight membrane with different salt retention properties and fouling propensity) are evaluated in order to investigate MIEX effectiveness under different fouling conditions and water chemistries. The main hypotheses to be tested are that MIEX may be deployed effectively to reduce fouling for different water-membrane systems and that operating conditions are critical to enhance effective interaction mechanism with HA. The latter aspect is of great importance to achieve fouling control under real water chemistries in NF sources for drinking water production.

2. Materials and Methods

2.1 Chemicals

The humic acid (HA, purchased from Sigma Aldrich, Germany) stock solution (500 mg/L) was prepared by dissolving 1.5 g of HA and 2.5 g NaOH in ultrapure water (pH 8) and stirring for 24 hours. The dissolved organic carbon (DOC) fraction was obtained by filtering the stock solution with a 0.45 μm PTFE (poly-tetra-fluoro-ethylene) filter. A buffer solution containing 2.5 mM $CaCl_2$ (Berndt Kraft, Germany), 1 mM $NaHCO_3$ (VWR Chemicals, Germany), 10 mM NaCl (VWR Chemicals, Germany), and 12.5 mgC/L of HA was used for the static adsorption experiments with MIEX as well as for membrane filtration experiments. HCl (1 M) and NaOH (1 M) were used to adjust the pH of the solutions varying from 2 to 10. Metabisulfite (Alfa Aesar, Germany) solution of 10 g/L was used to prevent bacterial growth on the used membrane. MilliQ water (MilliQ A+ system, Merck Millipore, Germany) was used to prepare solutions.

2.2 MIEX characteristics

Two types of MIEX resin beads ($MIEX_{DOC}$ and $MIEX_{GOLD}$) were provided by Orica Watercare (Melbourne, Australia). $MIEX_{DOC}$ and $MIEX_{GOLD}$ resins were compared in static adsorption experiments and only $MIEX_{DOC}$ were used in the filtration experiments. The main differences between the two resins, as reported by the supplier, are the rougher and higher surface area of $MIEX_{GOLD}$ and its larger pore openings, which allow easier access to inner bead area and increased exchange capacity, according to the manufacturer. For this reason, $MIEX_{GOLD}$ are able to remove low molecular weight organic material (< 5000 Da) compared with $MIEX_{DOC}$ [51]. Particle size and surface morphology of both resins were analyzed by environmental scanning electron microscopy (ESEM) and the micrographs are presented in the Supporting Information (see Figure S12). In these images, both resins display a porous and smooth surface. $MIEX_{GOLD}$ is heterogeneous in size and shape with larger particles ranging from roughly 50 μm to 400 μm. $MIEX_{DOC}$ appear more homogeneous with an average diameter of about140 μm, which is in accordance with values reported in the literature (150-180 μm) [52]. The Zeta potential of the resins was

measured at pH ranging from 2 to 10 and results are presented in Figure S13 of the Supporting Information. The resins showed slightly positive potentials at pH>6 (1-6 mV) while the zeta potential is close to zero at pH<6. This trend might be attributed to the high ionic conductance typical of ion exchange material, which significantly reduces the streaming potential signal and thus the magnitude of the measured zeta potential. Hence, measurement of streaming potential current were conducted in an electrolyte solution with similar electrical conductivity of that of the resin.

MIEX are usually acquired as a suspension having an organic content of 19 mgC/L. Therefore, a washing step was necessary prior to use in order to remove dissolved carbon-containing substances. The washing procedure was performed by diluting the MIEX with NaCl solution (1%) and mixing for 1 min. Subsequently, the resin was sedimented with a magnet, the supernatant removed, and the resin recovered. Finally, the resins were rinsed with MilliQ water and used for experiments.

2.3 Static adsorption tests of humic acid on MIEX resins

Static adsorption of HA on MIEX resins was investigated under different physico-chemical water conditions. The composition of the solutions used in the static adsorption study is summarized in Table 1.

Table 1. Buffer solution composition for the static adsorption experiments

Parameters	Concentration range (mM)	Buffer solution composition
$CaCl_2$	0-0.5-1-2.5- 3.5- 4	12.5 mgC/L HA, 10 mM NaCl, 1 mM $NaHCO_3$
NaCl	0.1-0.5-5-10-20-30-50	12.5 mg/L humic acid, 2.5 mM $CaCl_2$, 1 mM $NaHCO_3$
HA	4- 6-12.5-25-45 mgC/L	2.5 mM $CaCl_2$, 10 mM NaCl, 1mM $NaHCO_3$

Rinsed resins were settled for 5 minutes in a 10 mL syringe and 1.5 mL of suspension was added into a conical flask containing 150 mL of buffer solution to obtain a final resin concentration of 10 mL/L. Previous studies have shown that this concentration is optimal for NOM removal [53]. The flasks were shaken (New Brunswick™ Innova® 43) at the speed of 260 rpm for 60 min at 25 °C. MIEX adsorption was tested firstly for 4 hours: fast adsorption kinetics were observed and equilibrium was reached within 20 minutes (see Figure S15 in Supporting Information); therefore, 60 min was set as suitable time to evaluate static equilibrium adsorption. Samples of 10 mL were drawn at regular intervals for total organic carbon analysis. HA uptake (%) was calculated using Equation (1):

$$\text{HA uptake (\%)} = \left(1 - \frac{C_t}{C_i}\right) \cdot 100 \quad (1)$$

Where C_i (mg/L) is the initial HA concentration prior to resin addition, C_t (mg/L) is HA concentration at any given time, *t*. The mass of HA removed per mass of resin added, *Q* (mg/g), was calculated using Equation (2):

$$Q = \frac{(C_i - C_t) \cdot V_w}{M} \quad (2)$$

where V_w (L) is the solution volume at any given time, t, and M is the mass of resin added (g).

2.4 NF membranes

Two commercial NF membranes, NF270 and NF90 (provided as flat sheet samples by The Dow Chemical Company, Germany), were used for the fouling experiments. NF270 and NF90 consist of a semi-aromatic piperazine-based polyamide and a fully aromatic polyamide active layer, respectively [54]. The main properties of the membranes are summarized in Table 2.

Table 2. NF membrane characteristics used in the fouling experiments (MWCO= Molecular-weight-cut-off, IEP= isoelectric point, Lp= permeability)

Membrane	**MWCO (Da)**[*1]	**Ref.**	**IEP**	**Lp ($L\ m^{-2}h^{-1}bar^{-1}$)**	**Pore radius (nm)**[*2]	**Ref.**
NF90	90-180	[55-58]	~3.5	6 - 11	0.31-0.38	[56, 57, 59]
NF270	150-340	[55-57, 60]	~3	17-19	0.36-0.44	[56, 57, 61]

[*1,2] MWCO was determined by filtration of organic solutes (poly-ethylene glycol and sugars), pore size was estimated by applying the steric hindrance pore model

A new membrane coupon was used for each experiment; this coupon was soaked in NaCl 10 mM for 1 hour prior to use, then compacted by filtering MilliQ water at 9.6 bar for 1 hour. Soaking in NaCl enhances opening of the pores and swelling of the active layer due to interaction of electrolytes with the polyamide layer [62]. Normalized permeate flux (J_n) was calculated using Equation (3):

$$J_n = \frac{J_t}{J_{wo}} \quad (3)$$

The initial pure water flux, J_{wo} ($L\ m^{-2}h^{-1}$) was measured at steady-state before the filtration, while J_t ($L\ m^{-2}h^{-1}$) was the observed flux during fouling. The pure water flux was chosen as reference value due to practical limitations in the determination of a consistent value of flux in the presence of foulants at the very start of fouling experiments. The flux obtained by normalization with reference to J_{t0}, the flux at the beginning of the fouling experiment, is compared to the normalized permeate flux, J_n, in Figure S18 (Supporting Information). The filtration experiments were performed using a stainless steel stirred cell (capacity 900 mL) with an internal diameter of 7 cm, corresponding to an active membrane area of 38.48 cm^2. The cell was pressurized using synthetic compressed air that was supplied from the top of the cell.

The mass of permeate, as well as the feed pressure and the temperature, were monitored continuously and data were registered by using LabVIEW software (version 2014, National Instruments). A schematic representation of the system is reported in Figure 1.

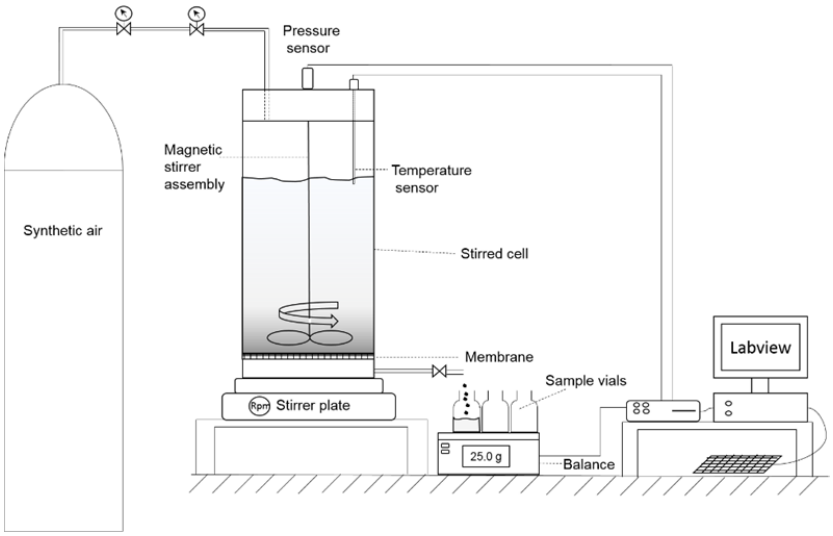

Figure 1. Stainless steel stirred cell system

For fouling experiments, 400 mL of feed solution containing HA (12.5 mgC/L), NaCl (10 mM), $NaHCO_3$ (1 mM), and $CaCl_2$ (2.5 mM), with or without a suspension of MIEX at 10 mL/L, was introduced into the cell and stirred at 400 rpm using a stirrer (model SU1300, Sunlab, Germany). Filtration was carried out at a trans-membrane pressure of 9.6 bar up to a recovery of 70 %. Nine permeate samples were collected during each test for a total volume of 280 mL and used for DOC analysis in order to measure the free HA concentration. HA retention was calculated using Equation (4):

$$R\ (\%) = \left(1 - \frac{C_p}{C_b}\right) \cdot 100 \qquad (4)$$

Where C_p (g/L) is HA concentration in the permeate, C_b (g/L) is HA concentration in the stirred cell, which changes over time and it is calculated as a function of permeate volume and concentration using Equation (5):

$$C_b = \frac{C_{FD} \cdot V_{FD} - \sum C_{Pi} \cdot V_{pi}}{V_R} \qquad (5)$$

where C_{FD} (g/L) is the initial HA concentration in the feed solution, C_{Pi} (g/L) is HA concentration in the permeate sample *i*, V_R (L) is the retentate volume (L), V_{FD} (L) is the initial feed volume, and V_{Pi} (L) is the permeate volume of sample *i*. After each fouling experiment, the cell containing the membrane was rinsed

gently with MilliQ water. The rinsing protocol consisted of filling the cell with MilliQ water (400 mL) without removing the membrane, rinsing manually and emptying. The rinsing was followed by evaluation of the pure water flux, J_W, by measuring steady-state permeation of MilliQ water at an applied pressure of 9.6 bar. The water flux reduction due to previous fouling, *FR*, was calculated using Equation (6):

$$\mathrm{FR}(\%) = \frac{\mathrm{J_{W0}} - \mathrm{J_W}}{\mathrm{J_{W0}}} \cdot 100 \qquad (6)$$

The fouled membrane samples were stored at 4 °C after treatment with sodium metabisulfite (10 g/L) in order to avoid bacterial growth prior to later imaging.

2.5 HA and IC analysis

HA and IC (inorganic carbon) concentrations in the solutions used for static adsorption tests, as well as in permeate, feed, and retentate samples of fouling tests, were measured with a GE Sievers M9 TOC Analyser (GE Analytical Instruments, UK). Feed and retentate samples were diluted 2 and 10 times, respectively, in order to ensure that concentrations were within the range of the calibration curve made with standard HA solutions (range 0-10 mgC/L). Samples were analyzed using an acid (H_2SO_4) and oxidizer (ammonium persulfate) flow rate of 1 µL/min.

2.6 Calcium analysis

Calcium concentration was measured by inductively coupled plasma optical emission spectrometry (ICP-OES, model Optima 8300DV, Perkin Elmer, Germany). Samples were diluted 10 times due to acidification with HNO_3 (5%) and treatment with Triton-X 100 before measurement.

2.7 Microscopy imaging

Environmental scanning electron microscopy (ESEM) (model Phillips ESEM-FEG XL30) was used to visualize MIEX resin beads morphology and particle surface. Fouling layer thickness was determined using scanning helium ion microscopy (HIM, ORION NanoFab, Carl Zeiss AG, Germany). The membrane samples were analyzed after the rinsing procedure explained in paragraph 2.4 in order to analyze only the material adsorbed irreversibly on the membrane surface. Cross-sections of the membrane discs were prepared manually using a sharp razor blade to minimize damage of the membrane surface. The HIM microscope was operated at an acceleration voltage and beam current of 30 kV and 0.3 pA, respectively, and the samples were imaged without any additional conductive coating with the aid of an electron flood gun.

2.8 Zeta potential analysis

The Zeta potential of MIEX beads and membranes was measured with an electrokinetic analyzer (SURPASS^{TM}, Anton Paar, Austria). The measurements of MIEX zeta potential were carried out with a background electrolyte solution of KCl (1 mM, VWR Chemicals, Germany) and at a temperature of 22 °C. The pH was adjusted using HCl or NaOH (50 mM). The MIEX bead powder was placed in a cylindrical measuring cell and the electrolyte solution flowed through the cell. An appropriate amount of powder was used in order to have a pressure of 200 mbar between the inlet and the outlet of the cylindrical cell and a flow rate in a range of 50 to 70 mL/min.

Zeta potential measurements of the membranes were carried in solutions containing NaCl only (15 mM), NaCl and HA, or in the same solutions used for fouling experiments that contained NaCl, $CaCl_2$, and HA. The method was similar to that described elsewhere [63]. Streaming potential measurements were carried out from at increasing pH starting from a value of 2 until a plateau in the magnitude of zeta potential was reached and no further change in potential was expected by increasing the pH of the solution.

3. Results and discussion

3.1 Comparison uptake of $MIEX_{DOC}$ and $MIEX_{GOLD}$ in static adsorption

Morphological analysis of $MIEX_{DOC}$ and $MIEX_{GOLD}$ resins revealed higher heterogeneity of particle size and shape of $MIEX_{GOLD}$ compared with $MIEX_{DOC}$ (see Figure S12of the Supporting Information). $MIEX_{GOLD}$ is characterized by higher ion exchange capacity according to the manufacturer. The adsorption of HA was investigated with both types of resin to determine their possible difference in performance and the sorption kinetics are reported in Figure 2.

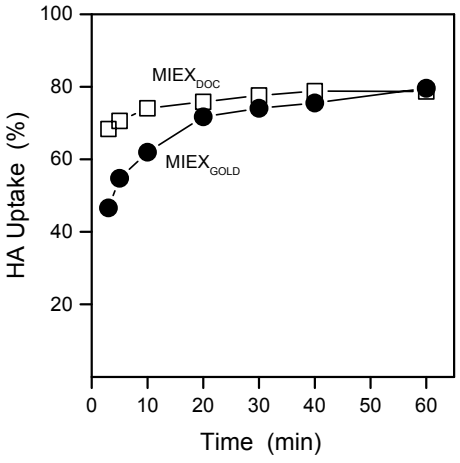

Figure 2. HA uptake (%) of two types of MIEX (12.5 mgC/L HA, 2.5 mM $CaCl_2$, 1 mM $NaHCO_3$, 10 mM NaCl, 10 mL/L MIEX, 150 mL, 20 °C, 260 rpm, pH 6)

Near steady-state was reached for both types of resin after about 20 min. Fast sorption kinetics resulted in uptake of more than 40% of the organic material after few minutes and 80% of organics at the end of the experiments. These data are consistent with adsorption driven by electrostatic attraction of negatively charged HA molecules and positively charged MIEX surfaces at pH 6 and are in accordance with previous reports [52, 64]. Overall, adsorption was slightly faster with $MIEX_{DOC}$ and this type of MIEX resin was thus chosen to conduct subsequent experiments.

3.2 Influence of HA concentration on HA-MIEX interaction

The variation of HA uptake at increased HA concentration was investigated to estimate the amount of HA adsorbed per unit mass of resin. This is relevant to understand HA-MIEX interaction in the dead-end stirred cell, where HA is concentrated within the cell during NF. HA uptake and specific mass adsorbed per mass of MIEX (Q) are reported in Figure 3a as a function of HA concentration. These data refer to the uptake at equilibrium (after 1 hour). HA uptake kinetics is reported in Figure S16 of theSupporting Information.

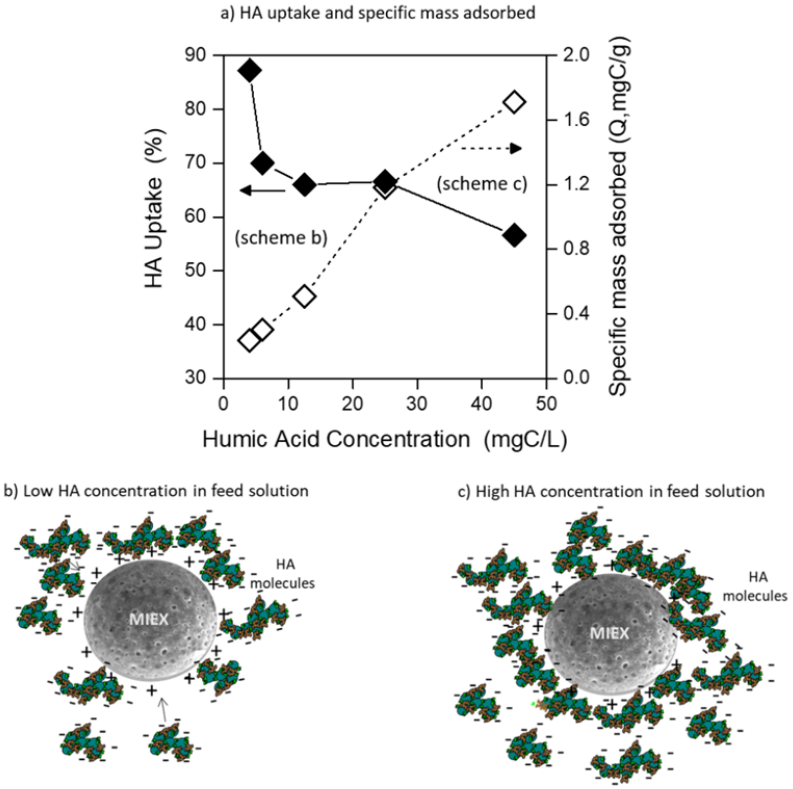

Figure 3. HA uptake and specific mass adsorbed of HA at increased HA concentration (12.5 mgC/L HA, 2.5 mM $CaCl_2$, 1 mM $NaHCO_3$, 10 mM NaCl, 10 mL/L MIEX, 150 mL, 20 °C, 260 rpm, pH 6, 60 min adsorption)

HA uptake decreased from 89 to 56 % with increasing HA concentration, while HA mass adsorbed per unit mass of MIEX increased clearly from 0.2 to 1.7 mgC/g. At low HA concentration, the MIEX surface remained available for adsorption until all available HA in solution was consumed (Figure 3b). In a middle range of HA concentrations, 6-25 mgC/L, HA uptake was constant at approximately 66% after 1 hour, independently of initial HA concentration in solution. Under these conditions, adsorption was not driven by interactions of suspended HA molecules with MIEX surfaces, but by interaction with already deposited HA molecules. This mechanism led to an increase of the overall amount of adsorbed HA (Figure 2c), even though the uptake did not change.

3.3 HA adsorption by MIEX as a function of water chemistry: ionic strength, hardness and pH

HA interactions with MIEX are mainly dominated by ion exchange mechanisms due to oppositely charged functional groups of HA molecules and MIEX surface. Thus, ionic strength, calcium concentration and pH are expected to play an important role by changing the charge density of HA molecules and by screening the electrostatic interactions. Furthermore, NaCl is used to regenerate saturated MIEX, based on the exchange of adsorbed materials with Cl^-. To promote regeneration, NaCl concentration is increased by one order of magnitude, based on the exchange capacity of 0.52 meq/mL [43]. 10 mL/L of MIEX corresponds to an exchange capacity of 5.2 meq/L (or 5.2 meq/L), therefore the regeneration concentration should be 50 mM, which was chosen in this study as highest ionic strength during experiments.

Ionic strength: a NaCl concentration range of 0 to 10 mM was chosen in order to determine when NaCl reduces HA uptake by MIEX and regeneration takes place. HA uptake as a function of NaCl concentration at equilibrium is reported in Figure 4a (HA uptake kinetic is reported in Figure S14 of the Supporting Information). Contrary to expectations, constant high HA uptake (about 65%) was observed with increasing NaCl concentration. Gosh *et al.* reported that HA molecules have a rigid sphero-colloid structure at high concentration of electrolytes and behave like uncharged polymers [65]. This effect appears to be dominant over the exchange mechanism at this concentration, thus allowing for denser packing of molecules on MIEX surface and resulting in higher adsorption values, as observed in other studies [66, 67]. Similar DOC removal was observed also by Apell *et al.* [43] during the regeneration process.

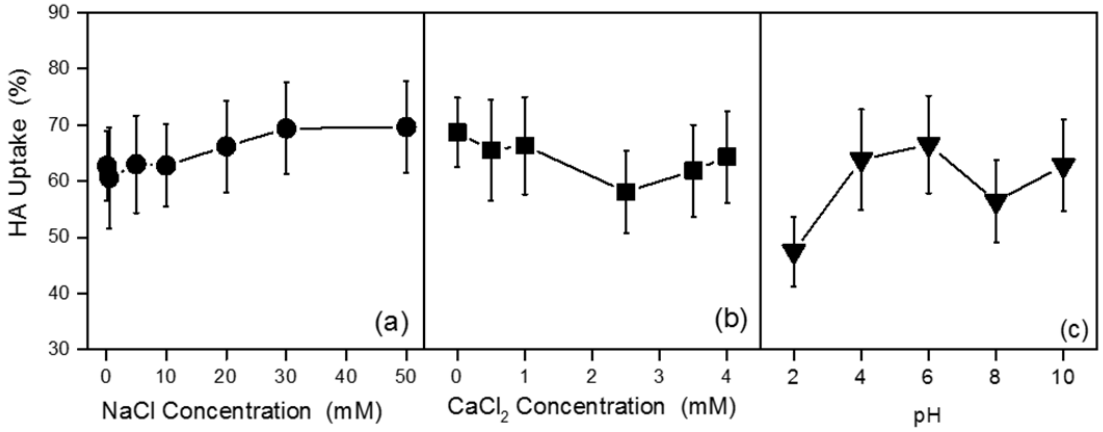

Figure 4. Effect of water chemistry on HA uptake after 60 min of adsorption: (a) ionic strength (2.5 mM $CaCl_2$, 12.5 mgC/L HA, 1 mM $NaHCO_3$, 10 mL/L MIEX), (b) calcium ($CaCl_2$) (10 mM NaCl, 12.5 mgC/L HA, 1 mM $NaHCO_3$, 10 mL/L MIEX), (c) pH (2.5 mM $CaCl_2$, 12.5 mgC/L HA, 10 mM NaCl, 1 mM $NaHCO_3$, 10 mL/L MIEX). 20 °C, 150 mL, 260 rpm.

Calcium concentration: In Figure 4b, HA uptake is reported as a function of $CaCl_2$ concentration. The range of calcium concentration was defined to investigate HA uptake in both soft (< 0.4 mM) and hard waters (≥ 4 mM). Calcium is ubiquitously present in drinking water. Tap and bottled water sources have a wide range of calcium concentration between 5 to above 200 mg/L (0.4-4.5 mM) [68]. Calcium ions interact strongly with the negatively charged groups of HA molecules reducing the electrostatic repulsion and the dissolution rate [25]. However, no significant change in HA uptake by MIEX was observed, suggesting that HA-MIEX interaction was not affected by calcium concentration.

pH: HA changes charge density, size and shape in different pH solutions [25, 69]. MIEX have a macroporous poly-acrylate shell with quaternary ammonium functional groups for ion exchange [64]. Ammonium (NH_4^+, pKa 9.25) is a strong base and is ionized completely in the pH range studied. The observed HA uptake as a function of pH is reported in Figure 4c. A slight increase from 47% to 66% was observed by increasing pH from 2 to 10. HA molecules contain mainly carboxyl and phenolic groups, which are deprotonated at pH 4-5 and pH 8-9, respectively [25]. At pH 2, charge density and dissolution rate of HA molecules is low, resulting in aggregation into molecular clusters [69]. These phenomena reduced the interaction with MIEX, leading to lower uptake. The increase of the negative charge density with increasing pH enhanced instead the interaction with the positively charged functional groups of MIEX resins and resulted in higher uptake. Taken together, results as a function of water composition suggested no significant effect of water chemistries on HA uptake due to stronger HA-MIEX interaction.

3.4 Flux decline during filtration in combined MIEX-NF process

Fouling studies were conducted using NF270 and NF90 membranes, which are loose and tight NF membranes, respectively. NaCl and $CaCl_2$ retention (without HA) is higher for NF90 (~85-90%) compared with NF270 (40-60%) [57, 58, 70], while both membranes have high HA rejection. This may be attributed to size exclusion of the high molecular weight compounds (measured retention was in the range 80-95% in this study, see Figure S17 of the Supporting Information). Calcium ions enhance NF membrane fouling by bridging the negative functional groups of the membrane surface with the HA molecules [26-29]. The pH of feed solution is also an important parameter affecting membrane-HA interaction, Ca-HA complexes, as well as HA-MIEX interactions [27, 31].

In Figure 5, flux decline at the end of the experiments in NF and combined MIEX-NF is reported as a function of pH for both membranes. Normalization of flux decline was carried out considering J_{w0}. Based on the rejection capabilities of the two types of membrane, a maximum loss in driving force of 10% and 16% due to concentration of feed solutes in the dead-end cell is estimated at the end of the tests with NF270 and NF90, respectively. The van't Hoff equation was used to calculate osmotic pressure from concentrate salt concentrations, which was then deducted from the applied pressure. Normalized flux declines below 0.9 and 0.84 for NF270 and NF90, respectively, should be attributable to fouling. Flux decline was more pronounced with NF90 membranes compared to NF270 membranes. However, the same trend with pH was observed, with higher decline in acidic (pH 2) and alkaline (pH 8, 10) solutions. At pH 2, the electrostatic repulsion between HA molecules and HA-membranes is reduced due to lower charge density of both materials. Therefore, deposition on the membrane surface of HA aggregates was promoted [22]. Lower flux declines were observed at pH 4 and 6, whereby carboxylic groups of both membranes and HA molecules are weakly ionized. Indeed, IEP of 3.5 was measured for NF90 and carboxyl groups of HA are deprotonated at pH 4-5. Brigante *et al.* observed that the dissolution rate of HA increases by more than two orders of magnitude by increasing the pH from 4 to 11 due to the disruption of hydrogen bonds between HA molecules [25]. As such, the lower flux decline might be attributed to weaker deposition of HA aggregates on the membrane. At higher pH values (8 and 10), the density of deprotonated carboxyl groups is higher and complexation of Ca-HA molecules becomes significant. Indeed, complexation of Ca-HA molecules as well as HA-membrane bridging have been reported to be stronger at high pH due to availability of more deprotonated carboxyl groups on both the membrane surface and HA molecules [12, 26]. As a result, highest flux declines were observed at pH 8 and 10 (normalized flux of 0.3 and 0.4 at the end of the test, respectively, for NF90 samples), corroborating the significant role of calcium ions in membrane fouling.

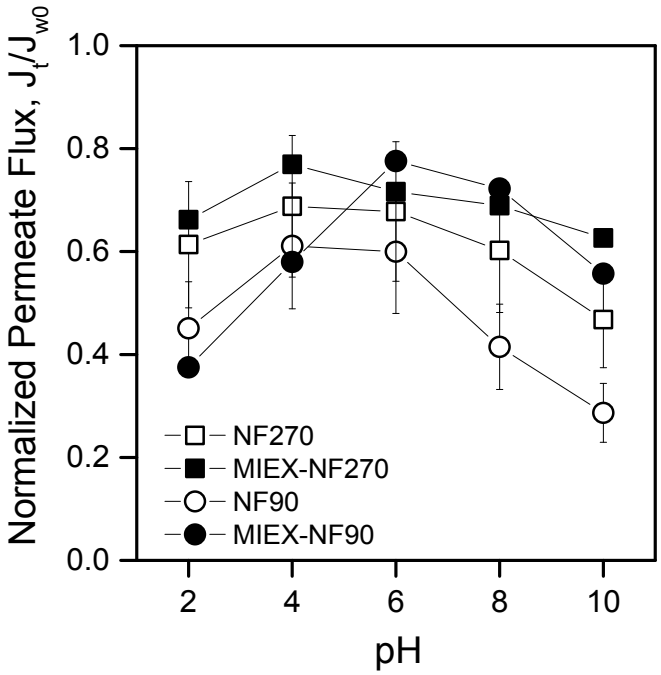

Figure 5. Normalized permeate flux as a function of pH (12.5 mg/L HA, 2.5 mM $CaCl_2$, 1 mM $NaHCO_3$, 10 mM NaCl, 10 mL/L MIEX, 9.6 bar, 400 rpm, 22 °C, 70% recovery)

At high pH, calcium can also contribute to membrane fouling by precipitation as calcite on the membrane surface and subsequent adsorption of HA molecules on the calcite. Schäfer *et al.* observed calcite formation at pH > 8 and 3 mM of calcium chloride [27]. In the present study, the initial feed solution contained 2.5 mM of calcium chloride and calcium concentration increased continuously in the stirred cell during filtration. Therefore, calcite precipitation is likely to occur at high rate at pH 10, resulting in severe flux decline (final normalized flux of 0.3 with NF90). This phenomenon may explain the lower decline observed with NF270 membranes (range of normalized flux 0.7-0.5), which are less capable of rejecting calcium (75% versus 98%). Membrane surface properties (e.g., hydrophobicity and roughness) contribute to membrane fouling. Boussu *et al.* reported that NF270 has higher hydrophilicity, smoother surface and higher charge density than NF90 [58]. However, contrasting results are present in the literature concerning fouling of NF270 and NF90. Some previous studies reported less fouling for NF270 compared to NF90 due to the smoother surface and higher hydrophilicity of the former membranes [24, 58]. On the contrary, other studies reported higher flux reduction for NF270 (33%) than NF90 (24%) due to its higher permeability, which resulted in greater initial flux when operating at the same applied pressure and hence higher concentration polarization [22]. Nghiem *et al.* identified calcium concentration as the major factor governing fouling by HA and similar flux decline was observed for both NF90 and NF270 at the same calcium concentration [71]. In this study,a larger flux decline was observed at high

pH values, where complexation and bridging Ca-HA with the membrane surface plays a major role in membrane fouling.

In the combined MIEX-NF process, system performance was improved. In the case of NF90, higher efficiency of MIEX addition was observed at high pH. Specifically, at pH 8 the final value of normalized flux increased from 0.4 to 0.7, while at pH 10 it increased from 0.3 to 0.6. This result is in accordance with the static adsorption study where higher HA uptake by MIEX was measured at high pH. The lower flux decline suggested that the presence of MIEX reduced the complexation of Ca-HA molecules and bridging or deposition onto the membrane surface. This is due to the stronger HA-MIEX interaction, which reduces the amount of free HA molecules to interact with calcium. MIEX effectiveness was low at acidic pH (2 and 4), as flux decline was only slightly reduced. According to the static adsorption tests, HA-MIEX interactions are weaker in acidic condition and HA molecules are mainly in the form of aggregates, which can deposit on the membrane surface during filtration, as discussed above.

In the case of NF270, the effect of MIEX addition was as significant as with the tighter membranes, resulting overall in significantly lower flux decline. The effect of MIEX was strongest at pH 10, with the final value of normalized flux increasing from 0.4 to 0.6 upon addition of MIEX. This result supports the hypothesis that the resin inhibited the adsorption of HA on the calcium precipitated onto the membrane surface due to stronger HA-MIEX interaction.

3.5 Flux reduction due to irreversible fouling in combined MIEX-NF process

Flux decline is an indication of loss of driving force, concentration polarization, and accumulation of organic material on the membrane surface (thus fouling) during operation. However, flux decline does not indicate whether fouling is reversible or irreversible. In the present study, the flux reduction, i.e., the loss of flux following fouling and rinsing of the membrane, was investigated to this purpose. Further, flux reduction in presence of MIEX was investigated at different pH values in order to evaluate optimal conditions for MIEX effectiveness. In Figure 6, pure water flux measured before and after the filtration of HA solution at different pH values is shown for both types of membrane in NF and combined MIEX NF processes.

High water flux reduction in a range between 53-78% was observed when NF90 was used without MIEX. Therefore, irreversible fouling was dominant, which was confirmed by the dark coloration of the membrane discs after rinsing, especially at alkaline pH values (8-10) (Figure 7). The results may be rationalized with the strong complexation of Ca-HA molecules on the membrane surface as mainly responsible of irreversible fouling during filtration by NF90. Lower water flux reduction (15-23%) was observed for NF270, independent of pH. This result suggests less irreversible fouling with the less

rejecting membrane. This is in agreement with the lower flux decline reported in Figure 5 as well as the cleaner membrane samples compared with NF90 after rinsing. The lower calcium retention reported in the literature for NF270 [57, 58, 70] as well as higher hydrophilicity and smoother surface [58] might explain the lower and reversible fouling observed with this membrane.

In the case of MIEX-NF90, the irreversible water flux reduction was 2 times lower (14-34%). Flux reduction of 34% was observed at pH 10, suggesting the inhibition of calcium effect by the resins: stronger interaction between MIEX and HA occurred, thus preventing calcium-organic complex formation. At pH 2, flux reduction was about 14%, in contrast with the high flux decline observed during filtration and reported above in Figure 5. This means that fouling was mostly reversible at pH 2. Indeed, HA aggregate deposits were bound weakly to the membrane and flux could be recovered by gentle rinsing with MilliQ water. This was supported by the qualitative analysis of the membrane disc, which did not appear heavily fouled at pH 2 following experiments conducted in the presence of MIEX (Figure 7). In the case of MIEX-NF270, the water flux was recovered fully after filtration, indicating that HA-MIEX interactions minimized HA layer deposition on the membrane. These results suggest that MIEX can effectively reduce irreversible fouling with both membranes.

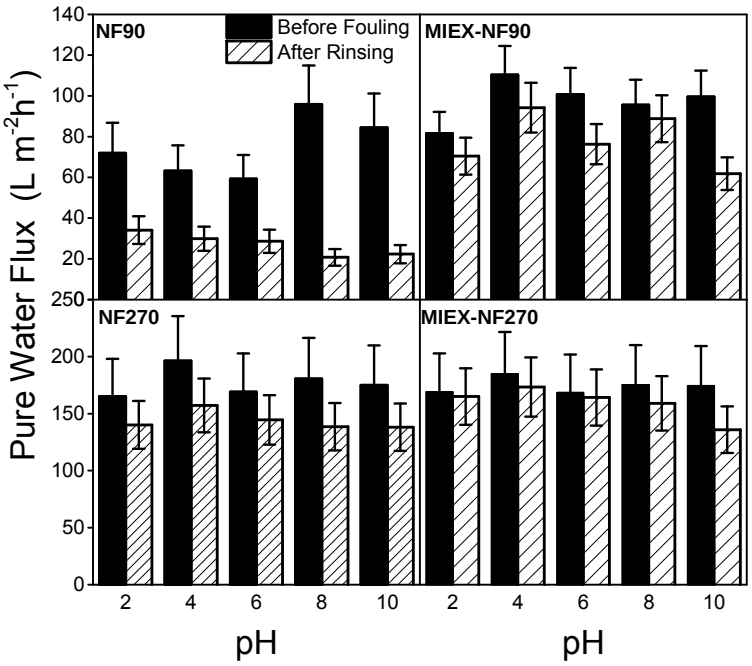

Figure 6. Water flux measured before and after filtration in NF and combined NF-MIEX at different pH values (12.5 mg/L HA, 2.5 mM $CaCl_2$, 1 mM $NaHCO_3$, 10 mM NaCl, 10 mL/L MIEX, 9.6 bar, 400 rpm, 22 °C, 70% recovery)

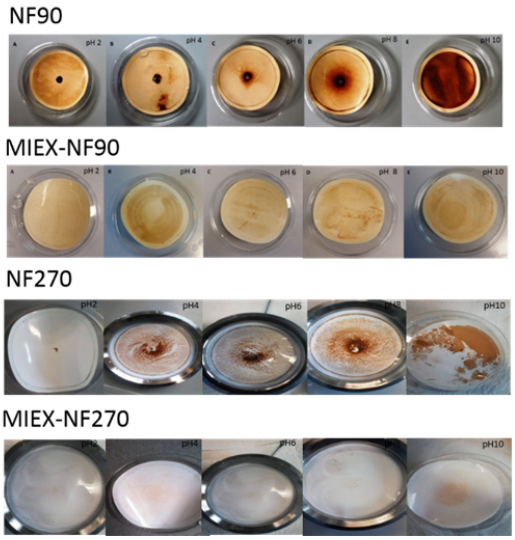

Figure 7. Appearance of the membrane discs after rinsing with MilliQ water

3.6 Impact of calcium on membrane zeta potential in fouling condition

The zeta potential of NF90 and NF270 in the presence of HA with and without calcium ions was measured in order to determine the impact of calcium on surface charge. Figure 8 summarizes zeta potential values measured in 15 mM NaCl, in HA solution, as well as HA+Ca solution.

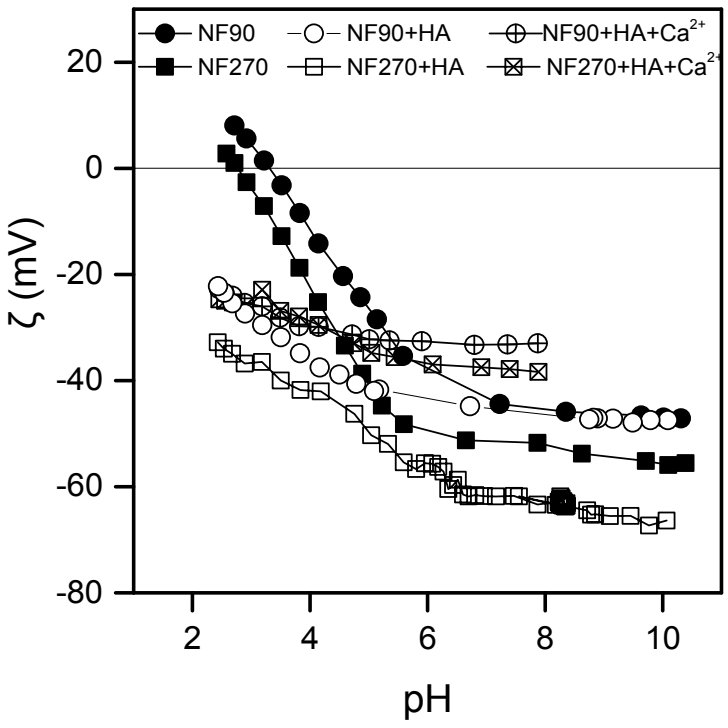

Figure 8. Zeta potential of NF270 and NF90 as a function of pH in different solutions containing (i) electrolytes only (NaCl 15 mM), (ii) electrolytes and HA (12.5 mgC/L HA, 1 mM NaHCO3, 10 mM NaCl), or (iii) electrolytes, HA and calcium (12.5 mgC/L HA, 1 mM $NaHCO_3$, 10 mM NaCl and 2.5 mM $CaCl_2$)

Comparison of the pristine membranes showed slightly higher negative charge of NF270 compared with NF90 and IEP of about 3-3.5, which was in accordance with other previous studies [63, 72]. The negative charge was related with deprotonation of the carboxylic group of the active polyamide layer [73]. The presence of HA increased the negative charge of both membranes over the entire pH range, indicating that interactions between HA and membranes occurred in both acidic and alkaline conditions. The same phenomenon was observed also in previous studies by streaming potential measurements [26, 74, 75]. HA molecules contain mainly carboxyl and phenolic groups, which are deprotonated at pH 4-5 and pH 8-9, respectively [25]. This explained the strong negative charge of the HA layer adsorbed on the membrane which dominates the membrane surface charge. As reported by Childress *et al.* [74, 75], HA adsorption on the membrane is mainly driven by hydrophobic interaction at higher pH values, where membrane and HA molecules are both negatively charged and electrostatic repulsion is present

In presence of calcium ions, a reduction in the magnitude of the zeta potential was observed for both NF90 and NF270, which can be correlated to the interaction of positively charged calcium ions with HA molecules at the membrane surface. This phenomenon appeared to be more pronounced for NF90 than NF270. These results contradict the results reported by Childress *et al.* [74] who observed an increase of the negative charge in presence of HA and calcium. This was attributed to higher HA adsorption due to complexation with calcium and bridging with the membrane surface. In another study by Hong *et al.* [26] a reduction of the negative membrane charge was observed by increasing calcium concentration in the presence of humic acid, which highlights the importance of the feed composition on the results obtained by streaming potential measurement. In the present study, the concentration of calcium is twice compared with the study carried out by Childress. Therefore, more calcium ions are available to interact with both negative functional groups of the membrane and functional groups of the adsorbed HA layer, thus reducing the overall magnitude of the negative potential.

In conclusion, the surface potential data supported the hypothesis that the complexation of Ca-HA molecules on the membrane surface was important in the fouling mechanism. This is in accordance with the previous results of flux decline and flux reduction that demonstrated major fouling under alkaline conditions.

4. Calcium and inorganic carbon (IC) retention in NF and combined NF-MIEX

Several studies suggest calcium as one of the main parameters responsible for membrane fouling by HA complexation and bridging with the membrane functional groups, especially at alkaline pH and with the

468 tighter NF membranes [21, 26-28, 30, 71]. Further, calcium interacts with carbonate species at alkaline
469 pH and precipitation of calcite occurs when the solubility limit of species is exceeded (what are those
470 solubility limit then you can estimate) [76]. Published studies reported higher retention of calcium by
471 NF90 (~85-90%) compared with NF270 (40-60%) in absence of organics [57, 58, 70], which is
472 correlated with different calcium concentration at the membrane/feed interface.

473 HA-Ca interaction is expected to increase calcium retention. In consequence, calcium and IC retention
474 was determined in presence of HA during fouling tests. In Figure 9, IC and calcium retention as a
475 function of pH is compared. High IC (75-97%) and calcium retention (92-98%) was determined for NF90
476 independent of pH, while low calcium (65-75%) and IC (75-89%) retention was observed for NF270 at
477 alkaline pH. The calcium concentration measured at the end of the tests after 70% recovery, reported in
478 Figure S20 (Supporting Information), was roughly 4 and 4.8 mM for NF270 and NF90, respectively.
479 Schäfer et al. observed precipitation of calcite at pH>8 and 3 mM $CaCl_2$ using a background solution of 1
480 mM $NaHCO_3$, 20 mM NaCl [27]. Concentration at the membrane/solution interface will be even higher
481 than the reported values due to concentration polarization and as recovery increases.

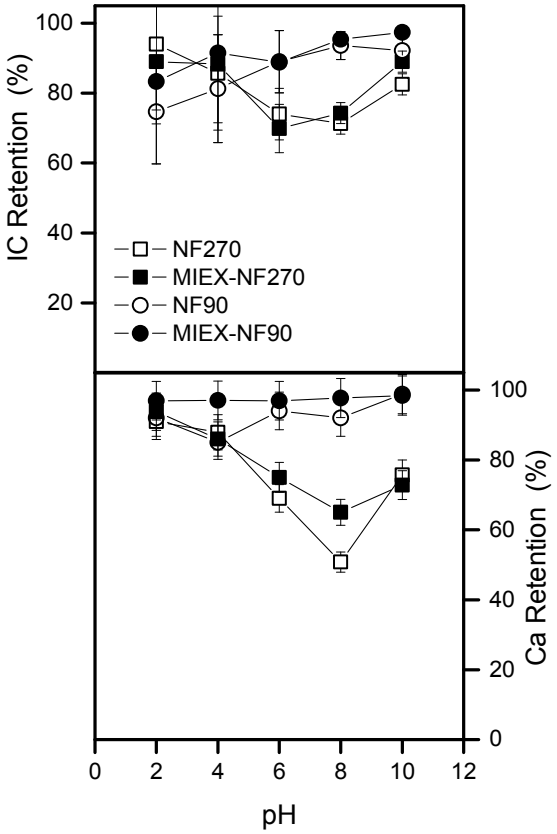

Figure 9. Calcium and IC retention as a function of pH (12.5 mg/L HA, 2.5 mM $CaCl_2$, 1 mM $NaHCO_3$, 10 mM NaCl, 10 mL/L MIEX, 9.6 bar, 400 rpm, 22 °C, 70% recovery)

Both membranes shown different response to pH changes, which may be rationalized with different retention mechanisms. For the tight NF90 membrane, retention of both carbonate species and calcium was not affected significantly by pH meaning that 1) there is no evident impact of carbonate speciation on retention, and 2) electrostatic repulsion is not the dominant retention mechanism of these species. Hydrated radius for Ca^{2+} and carbonate species (HCO_3^- and CO_3^{2-}) has been reported to be in a range of 0.26-0.41 nm [9, 77]and 0.26-0.39 nm [78, 79], respectively. NF90 has pore size in the range of 0.31-0.38 nm, suggesting that size exclusion is dominant in retaining carbonate and calcium. In contrast, for the NF270 membrane, charge repulsion appears to be significant. In fact, the highest calcium retention was observed at pH 2 and 4 (88-94%) due to the positive charge at the membrane surface (IEP 3). The lowest retention of both calcium (60-69 %) and IC (70-74%) was observed at pH 6 and 8 when the membrane is negatively charged. Calcium retention increased to 75% at pH 10 probably due to stronger complexation with the negatively charged HA molecules and precipitation of calcite. Similar trend for both calcium and IC is reported in other studies where membrane charge was demonstrated to play major role in solute

retention [9, 63]. Retention experiments imply that a larger concentration of calcium is present at the membrane solution/interface for tighter NF90 membranes than for looser NF270 membranes (how were you able to exclude flux effects?). In consequence, irreversible organic fouling, was more pronounced for the NF90.

A schematic is presented in Figure 10 to summarize the overall HA-Ca-membrane and HA-MIEX interactions that cause reversible or irreversible fouling under both alkaline and acid pH conditions. In acidic pH, Ca-HA interactions are negligible due to low HA charge density and fouling is mainly caused by deposition of HA aggregates, which only interact weakly with the membrane surface. Equally, HA-MIEX interaction is weak under acidic conditions, while aggregate deposits can be removed by water rinsing. At neutral to alkaline pH values, relevant for most water sources, HA-Ca complexation as well as calcium-mediated bridging with the membrane occur due to the negative charges of both membrane surfaces and HA molecules, resulting in irreversible deposits. This was more significant for the tight membrane leading to higher calcium concentrations at the membrane/solution interface. However, HA-MIEX interactions are stronger than Ca-HA interaction, resulting in less favourable HA layer deposition and lower irreversible fouling of the membrane when resins are present.

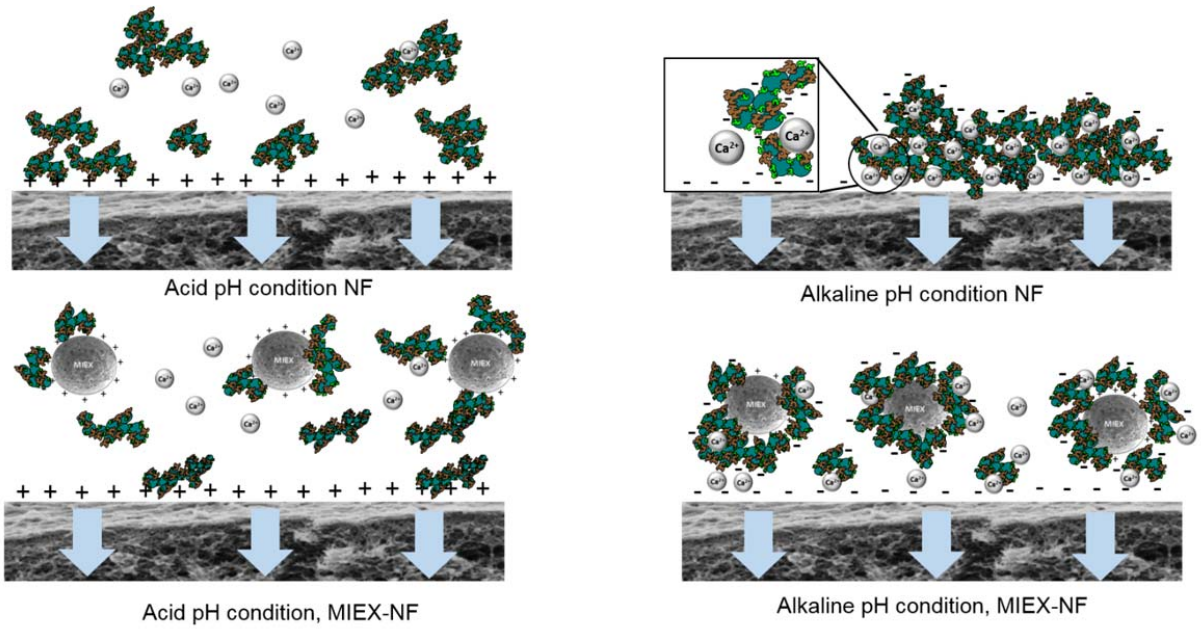

Figure 10. Schematic of HA-Ca-membranes and HA-MIEX interaction mechanisms HA-Ca-membranes and HA-MIEX in NF and combined NF-MIEX at alkaline and acidic pH condition

3.8 Impact of MIEX on fouling layer morphology analyzed using HIM (or HeIM)

To visualize the fouling layer thicknesses HIM analysis of membrane cross-section was performed. HIM microscope offers several benefits in terms of resolution, material contrast and surface sensitivity due to the unique physics of the interaction of moderate energy helium ions with material surfaces [80]. This offers the possibility to observe the membrane structure without conductive coating, which is instead necessary prior to traditional SEM analysis. Therefore, the fouling layer of HA deposited on the membrane could be preserved and imaged without artifacts resulting from such sample preparation. Figure 11 presents micrographs of the cross-sections of the pristine NF90 and NF270 membranes (Figure 11 A and B, respectively), the membranes fouled by HA at pH 8 without MIEX (Figure 11 C and D), and in the combined MIEX-NF process (Figure 11 E and F). Samples at pH 8 were selected as representative of natural water conditions. Both NF90 and NF270 are composed of a polyester support, polysulfone middle layer, and a thin polyamide active layer [81]. In Figure 11 A and B, the thin active layer and the porous substrate were clearly visible in the cross-sectional micrographs. NF90 was characterized by a rough surface while NF270 surface was much smoother, as reported also by Boussu *tr* [58]. A packed and dense deposited layer of HA is visible for NF90 and NF270 in Figure 11 C and D, respectively. However, in the case of NF90 (Figure 11 C), the fouling layer thickness was about 1.1 μm, while it was roughly 0.65 μm for NF270, that is, almost 2 times lower. The difference of fouling layer thickness confirmed the data discussed above showing significant flux decline and irreversible fouling for NF90 and less fouling for NF270. At neutral and alkaline pH, HA-Ca complexation enhanced the formation of a densely packed layer on the membrane surface and this effect is more significant for NF90. Moreover, membrane roughness has been reported to be an important parameter affecting fouling of NF membranes [17, 58]. Since NF270 is much smoother than NF90, less fouling has been reported in previous studies [24, 58] and this confirms the results obtained in this study where reversible fouling was observed for NF270. Figure 11 E and F displays membrane cross-section from the combined MIEX-NF. The densely packed layer of HA observed for fouled membranes in the single NF process was no longer present. In Figure 11 E, the membrane surface of NF90 was comparable with the pristine membrane, meaning that the fouling layer was mostly removed after the rinsing process. This is in agreement with the data discussed above showing low water flux reduction in the presence of MIEX (14-34%). In Figure 11F, the smoother surface of NF270 was apparent and no significant layer deposition was identified. These results corroborate the effectiveness of MIEX to reduce HA layer deposition on the membrane due to either reversible or irreversible fouling.

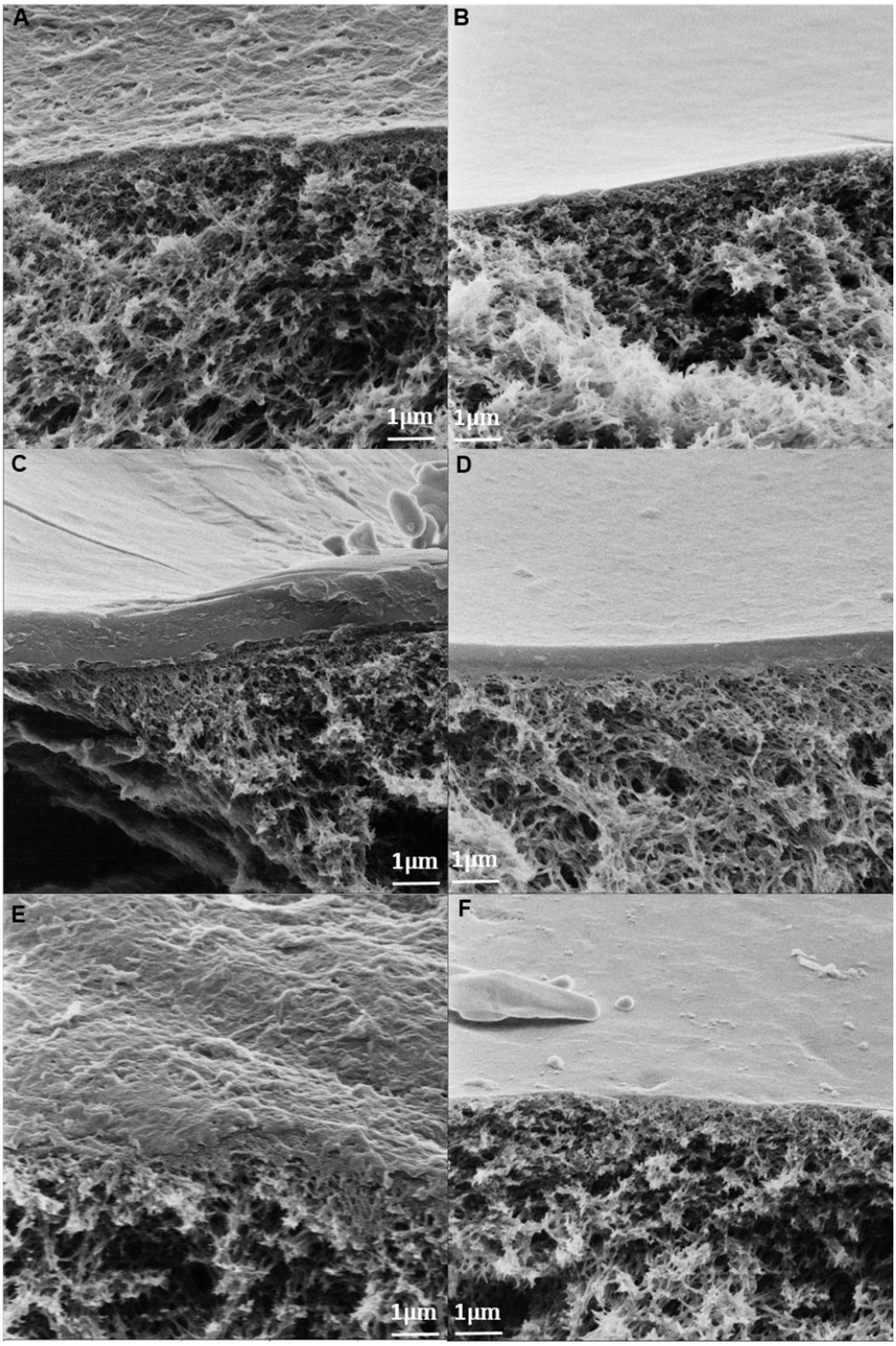

Figure 11. HIM micrographs of membrane cross-sections: A) clean NF90, B) clean NF270, C) fouled NF90 (pH 8), D) fouled NF270 (pH 8), E) fouled NF90-MIEX (pH 8), F) fouled NF270-MIEX (pH 8). Scale bar is 1 µm

551

552 **4. Conclusions**

553 Magnetic ion-exchange particles (MIEX) and nanofiltration (NF) were combined in one single process to
554 reduce fouling by humic acids (HA). MIEX effectiveness was investigated under different pH conditions
555 and with different membranes (tight and loose) in order to identify interaction mechanisms and optimal
556 operative conditions. Without MIEX, significant fouling by deposition of HA was observed, resulting in
557 high flux decline during operation (30-70%) and irreversible flux reduction (53-78%), especially with the
558 tight membrane (NF90). This phenomenon was more pronounced at alkaline pH: HA-Ca complexation
559 and bridging with the membrane were identified as the main phenomenon responsible for irreversible
560 membrane fouling. A dense and thickly packed HA fouling layer was characterized on the membrane by
561 He-microscope following these experiments. Lower but significant fouling was observed for the looser
562 membrane (NF270) in the absence of MIEX: in this case, the flux decline was 20-50%, and fouling was
563 mostly reversible, as pure water flux reduction after rinsing was 15-23%. These results were confirmed
564 by a fouling layer thickness 2 times lower compared with the deposited layer observed for NF90.

565 One of the main reasons for the different fouling behavior of the two membranes was their different
566 calcium retention. Calcium plays a major role in fouling of the membrane as interaction with HA
567 molecules and membrane surface is stronger in its presence. Calcium retention by NF90 was $> 95\%$,
568 independently of pH, while lower calcium retention (65-75%) was reported for NF270 at neutral to
569 alkaline pH. This implies a larger concentration of the divalent cation at the membrane/solution interface
570 for the tighter membrane, especially at high recovery rates, thus explaining the larger fouling observed
571 with NF90.

572 In the combined MIEX-NF, fouling was significantly reduced, resulting in both lower flux decline during
573 operation and lower irreversible loss of flux. In particular, irreversible flux reduction decreased
574 significantly for NF90, and water flux was fully recovered with NF270. Strong HA-MIEX interactions
575 were especially effective in minimizing calcium complexation and HA layer deposition at neutral and
576 alkaline pH, relevant for real applications. Results demonstrated the effectiveness of MIEX to minimize
577 fouling of NF membrane with different feed chemical compositions and the possibility to apply these
578 resins directly in the membrane system, minimizing or possibly eliminating any feed pre-treatment. This
579 is of great importance considering the wide variability of real water chemistries of sources tapped for
580 drinking water production by NF. Further, addition of MIEX may be an interesting application in tubular
581 or hollow fibre systems as well.

582 **5. Acknowledgments**

Helmholtz Association Rekrutierungs initiative and Politecnico di Torino are thanked for funding of the research at KIT and scholarship for SA respectively. The DOW Chemical Company and Orica Watercare (Australia) kindly supplied the membrane samples and MIEX resins respectively. Karlsruhe Nano Micro Facility (KNMF, www.knmf.kit.edu) is thanked for provision of access to the HIM microscope, Mohammed Taweheed (IFG, KIT) performed ESEM analysis, Prantik Samanta (KIT) performed the filtration experiments with NF270, Marita Heinle (KIT) is thanked for technical support with TOC analyzer and performing of calcium analysis, Matthias Franzreb is thanked for technical support with MIEX.

6. References

[1] S. Metsämuuronen, M. Sillanpää, A. Bhatnagar, M. Mänttäri, Natural Organic Matter Removal from Drinking Water by Membrane Technology, Sep. Purif. Rev., 43 (2014) 1-61.
[2] R. Liikanen, I. Miettinen, R. Laukkanen, Selection of NF membrane to improve quality of chemically treated surface water, Water Research, 37 (2003) 864-872.
[3] W.L. Ang, A.W. Mohammad, N. Hilal, C.P. Leo, A review on the applicability of integrated/hybrid membrane processes in water treatment and desalination plants, Desalination, 363 (2015) 2-18.
[4] Y. Zhang, N. Zhang, P. Zhao, Z. Niu, Characteristics of molecular weight distribution of dissolved organic matter in bromide-containing water and disinfection by-product formation properties during treatment processes, J. Environ. Sci., (2017) 1-11.
[5] R. Sadiq, M.J. Rodriguez, Disinfection by-products (DBPs) in drinking water and predictive models for their occurrence: a review, Science of The Total Environment, 321 (2004) 21-46.
[6] H. Komulainen, Experimental cancer studies of chlorinated by-products, Toxicology, 198 (2004) 239-248.
[7] C.G. Graves, G.M. Matanoski, R.G. Tardiff, Weight of Evidence for an Association between Adverse Reproductive and Developmental Effects and Exposure to Disinfection By-products: A Critical Review, Regulatory Toxicology and Pharmacology, 34 (2001) 103-124.
[8] S.D. Richardson, M.J. Plewa, E.D. Wagner, R. Schoeny, D.M. DeMarini, Occurrence, genotoxicity, and carcinogenicity of regulated and emerging disinfection by-products in drinking water: a review and roadmap for research, Mut. Res. Rev. Mut. Res., 636 (2007) 178-242.
[9] A.I. Schäfer, A. Pihlajamäki, A.G. Fane, T.D. Waite, M. Nyström, Natural organic matter removal by nanofiltration: effects of solution chemistry on retention of low molar mass acids versus bulk organic matter, J. Membr. Sci., 242 (2004) 73-85.
[10] C. Jarusutthirak, S. Mattaraj, R. Jiraratananon, Factors affecting nanofiltration performances in natural organic matter rejection and flux decline, Separation and Purification Technology, 58 (2007) 68-75.
[11] J. Shen, A.I. Schäfer, Factors affecting fluoride and natural organic matter (NOM) removal from natural waters in Tanzania by nanofiltration/reverse osmosis, Science of The Total Environment, 527 (2015) 520-529.
[12] A.S. Al-Amoudi, Factors affecting natural organic matter (NOM) and scaling fouling in NF membranes: A review, Desalination, 259 (2010) 1-10.
[13] A. Al-Amoudi, R.W. Lovitt, Fouling strategies and the cleaning system of NF membranes and factors affecting cleaning efficiency, J. Membr. Sci., 303 (2007) 4-28.
[14] A.W. Zularisam, A.F. Ismail, R. Salim, Behaviours of natural organic matter in membrane filtration for surface water treatment — a review, Desalination, 194 (2006) 211-231.

[15] A. Schäfer, N. Andritsos, A.J. Karabelas, E. Hoek, R. Schneider, M. Nyström, Fouling in nanofiltration, in: Nanofiltration – Principles and Applications, Elsevier, Great Britain, 2004, pp. 169-239.
[16] E.M. Vrijenhoek, S. Hong, M. Elimelech, Influence of membrane surface properties on initial rate of colloidal fouling of reverse osmosis and nanofiltration membranes, J. Membr. Sci., 188 (2001) 115-128.
[17] G.Z. Ramon, E.M. Hoek, Transport through composite membranes, part 2: Impacts of roughness on permeability and fouling, J. Membr. Sci., 425 (2013) 141-148.
[18] G.Z. Ramon, M.C. Wong, E.M. Hoek, Transport through composite membrane, part 1: Is there an optimal support membrane?, J. Membr. Sci., 415 (2012) 298-305.
[19] A.E. Contreras, Z. Steiner, J. Miao, R. Kasher, Q. Li, Studying the role of common membrane surface functionalities on adsorption and cleaning of organic foulants using QCM-D, Environ. Sci. Tech., 45 (2011) 6309-6315.
[20] A. Braghetta, F.A. DiGiano, W.P. Ball, NOM accumulation at NF membrane surface: impact of chemistry and shear, J. Environ. Eng., 124 (1998) 1087-1098.
[21] A. Seidel, M. Elimelech, Coupling between chemical and physical interactions in natural organic matter (NOM) fouling of nanofiltration membranes: implications for fouling control, J. Membr. Sci., 203 (2002) 245-255.
[22] C.Y. Tang, Y.-N. Kwon, J.O. Leckie, Fouling of reverse osmosis and nanofiltration membranes by humic acid—effects of solution composition and hydrodynamic conditions, J. Membr. Sci., 290 (2007) 86-94.
[23] E.M. Hoek, A.S. Kim, M. Elimelech, Influence of crossflow membrane filter geometry and shear rate on colloidal fouling in reverse osmosis and nanofiltration separations, Environ. Eng. Sci., 19 (2002) 357-372.
[24] C.Y. Tang, J.O. Leckie, Membrane independent limiting flux for RO and NF membranes fouled by humic acid, Environ. Sci. Tech., 41 (2007) 4767-4773.
[25] M. Brigante, G. Zanini, M. Avena, On the dissolution kinetics of humic acid particles: effects of pH, temperature and Ca2+ concentration, Coll. Surf. A: Physicochem. Eng. Asp., 294 (2007) 64-70.
[26] S. Hong, M. Elimelech, Chemical and physical aspects of natural organic matter (NOM) fouling of nanofiltration membranes, J. Membr. Sci., 132 (1997) 159-181.
[27] A.I. Schäfer, A.G. Fane, T.D. Waite, Nanofiltration of natural organic matter: Removal, fouling and the influence of multivalent ions, Desalination, 118 (1998) 109-122.
[28] W.S. Ang, A. Tiraferri, K.L. Chen, M. Elimelech, Fouling and cleaning of RO membranes fouled by mixtures of organic foulants simulating wastewater effluent, J. Membr. Sci., 376 (2011) 196-206.
[29] A.I. Schäfer, A.G. Fane, T.D. Waite, Fouling effects on rejection in the membrane filtration of natural waters, Desalination, 131 (2000) 215-224.
[30] E.E. Chang, Y.-C. Chang, C.-H. Liang, C.-P. Huang, P.-C. Chiang, Identifying the rejection mechanism for nanofiltration membranes fouled by humic acid and calcium ions exemplified by acetaminophen, sulfamethoxazole, and triclosan, Journal of Hazardous Materials, 221 (2012) 19-27.
[31] T. Wang, Y.-J. Yen, Y.-K. Hsieh, J. Wang, Size effect of calcium-humic acid non-rigid complexes on the fouling behaviors in nanofiltration: An LA-ICP-MS study, Coll. Surf. A: Physicochem. Eng. Asp., 513 (2017) 335-347.
[32] Y. Mo, A. Tiraferri, N.Y. Yip, A. Adout, X. Huang, M. Elimelech, Improved antifouling properties of polyamide nanofiltration membranes by reducing the density of surface carboxyl groups, Environ. Sci. Tech., 46 (2012) 13253-13261.
[33] S. Van Geluwe, L. Braeken, B. Van der Bruggen, Ozone oxidation for the alleviation of membrane fouling by natural organic matter: A review, Water Research, 45 (2011) 3551-3570.
[34] W. Song, V. Ravindran, B.E. Koel, M. Pirbazari, Nanofiltration of natural organic matter with H 2 O 2/UV pretreatment: fouling mitigation and membrane surface characterization, J. Membr. Sci., 241 (2004) 143-160.

[35] H. Shon, S. Vigneswaran, R.B. Aim, H. Ngo, I.S. Kim, J. Cho, Influence of flocculation and adsorption as pretreatment on the fouling of ultrafiltration and nanofiltration membranes: application with biologically treated sewage effluent, Environ. Sci. Tech., 39 (2005) 3864-3871.
[36] T. Bond, E. Goslan, S. Parsons, B. Jefferson, Disinfection by-product formation of natural organic matter surrogates and treatment by coagulation, MIEX® and nanofiltration, Water research, 44 (2010) 1645-1653.
[37] T. Carroll, S. King, S. Gray, B.A. Bolto, N. Booker, The fouling of microfiltration membranes by NOM after coagulation treatment, Water Research, 34 (2000) 2861-2868.
[38] C. Stoquart, P. Servais, P.R. Bérubé, B. Barbeau, Hybrid Membrane Processes using activated carbon treatment for drinking water: A review, J. Membr. Sci., 411 (2012) 1-12.
[39] J. Kaewsuk, G.T. Seo, Verification of NOM removal in MIEX-NF system for advanced water treatment, Separation and Purification Technology, 80 (2011) 11-19.
[40] E. Cornelissen, D. Chasseriaud, W. Siegers, E. Beerendonk, D. Van der Kooij, Effect of anionic fluidized ion exchange (FIX) pre-treatment on nanofiltration (NF) membrane fouling, Water research, 44 (2010) 3283-3293.
[41] H. Son, Y. Hwang, J. Roh, K. Ji, P. Sin, C. Jung, L. Kang, Application of MIEX® pre-treatment for ultrafiltration membrane process for NOM removal and fouling reduction, Water Sci. Tech.: Water Supp., 5 (2005) 15-24.
[42] X. Zhang, F. Li, X. Zhao, Application of a magnetic resin (MIEX®) in wastewater reclamation for managed aquifer recharge, Water Air and Soil Pollution, 223 (2012) 4687-4694.
[43] J.N. Apell, T.H. Boyer, Combined ion exchange treatment for removal of dissolved organic matter and hardness, Water Research, 44 (2010) 2419-2430.
[44] T.V. Nguyen, R. Zhang, S. Vigneswaran, H.H. Ngo, J. Kandasamy, P. Mathes, Removal of organic matter from effluents by Magnetic Ion Exchange (MIEX®), Desalination, 276 (2011) 96-102.
[45] T.H. Boyer, Removal of Dissolved Organic Matter by Magnetic Ion Exchange Resin, Curr. Poll. Rep., 1 (2015) 142-154.
[46] T.H. Boyer, P.C. Singer, Bench-scale testing of a magnetic ion exchange resin for removal of disinfection by-product precursors, Water Research, 39 (2005) 1265-1276.
[47] D.A. Fearing, J. Banks, S. Guyetand, C.M. Eroles, B. Jefferson, D. Wilson, P. Hillis, A.T. Campbell, S.A. Parsons, Combination of ferric and MIEX® for the treatment of a humic rich water, Water Research, 38 (2004) 2551-2558.
[48] A. Aryal, A. Sathasivan, Importance of the order in enhancing EfOM removal by combination of BAC and MIEX®, Water Science and Technology, 64 (2011) 2325-2332.
[49] A. Aryal, A. Sathasivan, A. Heitz, G. Zheng, H. Nikraz, M.P. Ginige, Combined BAC and MIEX pre-treatment of secondary wastewater effluent to reduce fouling of nanofiltration membranes, water research, 70 (2015) 214-223.
[50] H.J. Son, Y.D. Hwang, J.S. Roh, K.W. Ji, P.S. Sin, C.W. Jung, L.S. Kang, Application of MIEX® pre-treatment for ultrafiltration membrane process for NOM removal and fouling reduction, Water Sci. Tech.: Water Supp., 5 (2005) 15-24.
[51] I. Watercare, in.
[52] M. Kitis, B. İlker Harman, N.O. Yigit, M. Beyhan, H. Nguyen, B. Adams, The removal of natural organic matter from selected Turkish source waters using magnetic ion exchange resin (MIEX®), Reactive and Functional Polymers, 67 (2007) 1495-1504.
[53] H. Humbert, H. Gallard, H. Suty, J.-P. Croué, Performance of selected anion exchange resins for the treatment of a high DOC content surface water, Water Research, 39 (2005) 1699-1708.
[54] M. Mänttäri, T. Pekuri, M. Nyström, NF270, a new membrane having promising characteristics and being suitable for treatment of dilute effluents from the paper industry, J. Membr. Sci., 242 (2004) 107-116.

[55] E. Sjöman, M. Mänttäri, M. Nyström, H. Koivikko, H. Heikkilä, Separation of xylose from glucose by nanofiltration from concentrated monosaccharide solutions, J. Membr. Sci., 292 (2007) 106-115.
[56] L.D. Nghiem, A.I. Schäfer, M. Elimelech, Removal of natural hormones by nanofiltration membranes: measurement, modeling, and mechanisms, Environ. Sci. Tech., 38 (2004) 1888-1896.
[57] M.J. López-Muñoz, A. Sotto, J.M. Arsuaga, B. Van der Bruggen, Influence of membrane, solute and solution properties on the retention of phenolic compounds in aqueous solution by nanofiltration membranes, Separation and Purification Technology, 66 (2009) 194-201.
[58] K. Boussu, Y. Zhang, J. Cocquyt, P. Van Der Meeren, A. Volodin, C. Van Haesendonck, J. Martens, B. Van der Bruggen, Characterization of polymeric nanofiltration membranes for systematic analysis of membrane performance, J. Membr. Sci., 278 (2006) 418-427.
[59] A. Simon, J.A. McDonald, S.J. Khan, W.E. Price, L.D. Nghiem, Effects of caustic cleaning on pore size of nanofiltration membranes and their rejection of trace organic chemicals, J. Membr. Sci., 447 (2013) 153-162.
[60] K. Boussu, J. De Baerdemaeker, C. Dauwe, M. Weber, K.G. Lynn, D. Depla, S. Aldea, I.F. Vankelecom, C. Vandecasteele, B. Van der Bruggen, Physico-chemical characterization of nanofiltration membranes, Chem. Phys. Chem., 8 (2007) 370-379.
[61] H.Q. Dang, W.E. Price, L.D. Nghiem, The effects of feed solution temperature on pore size and trace organic contaminant rejection by the nanofiltration membrane NF270, Separation and Purification Technology, 125 (2014) 43-51.
[62] M. Nilsson, G. Trägårdh, K. Östergren, The influence of sodium chloride on mass transfer in a polyamide nanofiltration membrane at elevated temperatures, J. Membr. Sci., 280 (2006) 928-936.
[63] I. Owusu-Agyeman, A. Jeihanipour, T. Luxbacher, A.I. Schäfer, Implications of humic acid, inorganic carbon and speciation on fluoride retention mechanisms in nanofiltration and reverse osmosis, J. Membr. Sci., 528 (2017) 82-94.
[64] P.C. Singer, K. Bilyk, Enhanced coagulation using a magnetic ion exchange resin, Water Research, 36 (2002) 4009-4022.
[65] K. Ghosh, M. Schnitzer, Macromolecular structures of humic substances, Soil Sci., 129 (1980) 266-276.
[66] C. Shuang, F. Pan, Q. Zhou, M. Zhang, A. Li, P. Li, Adsorption of HA Fractions with Different Molecular Weight on Magnetic Polyacrylic Anion Exchange Res, in: Functional of Natural Organic Matter in Changing Environment, Springer, 2013, pp. 177-180.
[67] A. Tiraferri, L.A.S. Hernandez, C. Bianco, T. Tosco, R. Sethi, Colloidal behavior of goethite nanoparticles modified with humic acid and implications for aquifer reclamation, Journal of Nanoparticle Research, 19 (2017) 107.
[68] A. Azoulay, P. Garzon, M.J. Eisenberg, Comparison of the mineral content of tap water and bottled waters, J. Gen. Intern. Med., 16 (2001) 168-175.
[69] C. Colombo, G. Palumbo, R. Angelico, H.G. Cho, O. Francioso, A. Ertani, S. Nardi, Spontaneous aggregation of humic acid observed with AFM at different pH, Chemosphere, 138 (2015) 821-828.
[70] G. Bargeman, J.B. Westerink, C.F.H. Manuhutu, A.t. Kate, The effect of membrane characteristics on nanofiltration membrane performance during processing of practically saturated salt solutions, J. Membr. Sci., 485 (2015) 112-122.
[71] L.D. Nghiem, D. Vogel, S. Khan, Characterising humic acid fouling of nanofiltration membranes using bisphenol A as a molecular indicator, Water Research, 42 (2008) 4049-4058.
[72] C.Y. Tang, Y.-N. Kwon, J.O. Leckie, Characterization of humic acid fouled reverse osmosis and nanofiltration membranes by transmission electron microscopy and streaming potential measurements, Environ. Sci. Tech., 41 (2007) 942-949.

[73] M. Mänttäri, A. Pihlajamäki, M. Nyström, Effect of pH on hydrophilicity and charge and their effect on the filtration efficiency of NF membranes at different pH, Journal of Membrane Science, 280 (2006) 311-320.
[74] A.E. Childress, M. Elimelech, Effect of solution chemistry on the surface charge of polymeric reverse osmosis and nanofiltration membranes, Journal of Membrane Science, 119 (1996) 253-268.
[75] A.E. Childress, M. Elimelech, Relating Nanofiltration Membrane Performance to Membrane Charge (Electrokinetic) Characteristics, Environmental Science & Technology, 34 (2000) 3710-3716.
[76] A. Antony, J.H. Low, S. Gray, A.E. Childress, P. Le-Clech, G. Leslie, Scale formation and control in high pressure membrane water treatment systems: a review, J. Membr. Sci., 383 (2011) 1-16.
[77] I. Danielewicz-Ferchmin, A.R. Ferchmin, Mass density in hydration shells of ions, Physica B: Condensed Matter, 245 (1998) 34-44.
[78] A.M. Kiss, T.D. Myles, K.N. Grew, A.A. Peracchio, G.J. Nelson, W.K.S. Chiu, Carbonate and Bicarbonate Ion Transport in Alkaline Anion Exchange Membranes, Journal of The Electrochemical Society, 160 (2013) F994-F999.
[79] E.R. Nightingale, Phenomenological theory of ion solvation. Effective radii of hydrated ions, The Journal of Physical Chemistry, 63 (1959) 1381-1387.
[80] L. Scipioni, Principles and applications of helium ion microscopy, in, 2009.
[81] E.I. Mouhoumed, A. Szymczyk, A. Schäfer, L. Paugam, Y.-H. La, Physico-chemical characterization of polyamide NF/RO membranes: insight from streaming current measurements, J. Membr. Sci., 461 (2014) 130-138.
[82] B. Lenntech, Water Conductivity, in, 2017.
[83] A. Almansoori, Y. Saif, Structural optimization of osmosis processes for water and power production in desalination applications, Desalination, 344 (2014) 12-27.

Organic Fouling through Magnetic Ion Exchange-Nanofiltration (MIEX-NF) in Water Treatment

Alessandra Imbrogno[a]*, Alberto Tiraferri[b], Sara Abbenante[a,b], Stephan Weyand[c], Ruth Schwaiger[c,d], Thomas Luxbacher[e], Andrea I. Schäfer[a]

[a] Membrane Technology Department, Institute of Functional Interfaces, Karlsruhe Institute of Technology (KIT), Hermann-von-Helmholtz-Platz 1, 76344 Eggenstein-Leopoldshafen, Germany

[b] Department of Environment, Land and Infrastructure Engineering (DIATI), Politecnico di Torino, Turin, Italy, Corso Duca degli Abruzzi 24, 10129, Turin, Italy

[c] Institute for Applied Materials, Karlsruhe Institute of Technology (KIT), Hermann-von-Helmholtz-Platz 1, 76344 Eggenstein-Leopoldshafen, Germany

[d] Karlsruhe Nano Micro Facility (KNMF), Karlsruhe Institute of Technology (KIT), Hermann-von-Helmholtz-Platz 1, 76344 Eggenstein-Leopoldshafen, Germany

[e] Anton Paar GmbH, Anton-Paar-Str. 20, 8054 Graz, Austria

SUPPORTING INFORMATION

1. ESEM characterization of $MIEX_{DOC}$ and $MIEX_{GOLD}$

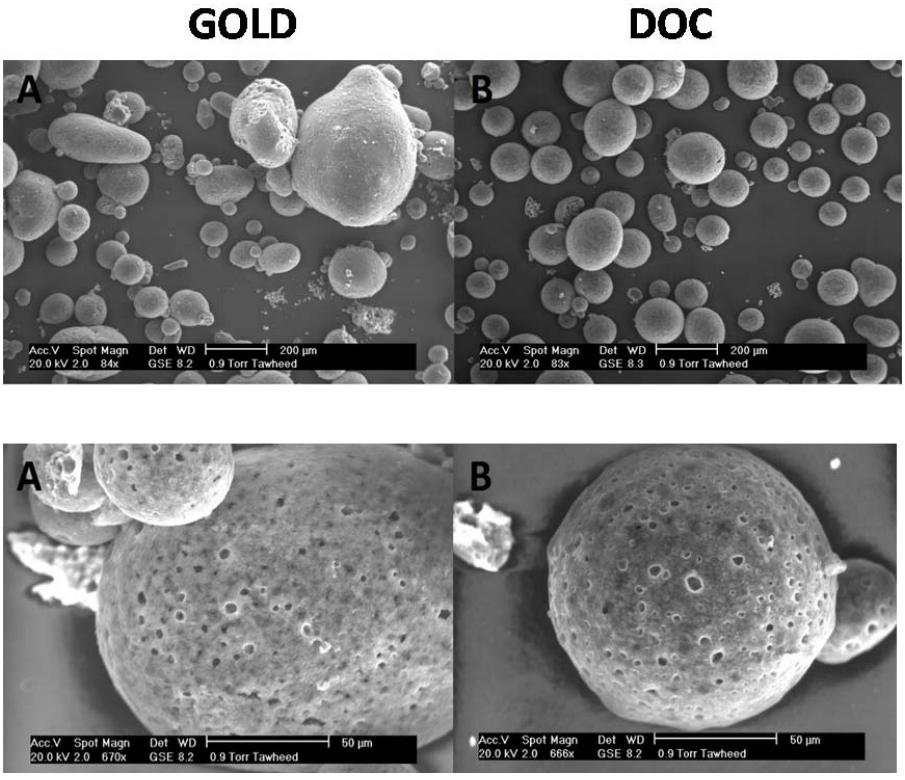

Figure S12. ESEM micrographs of (A) $MIEX_{GOLD}$ and (B) $MIEX_{DOC}$ at different magnifications.

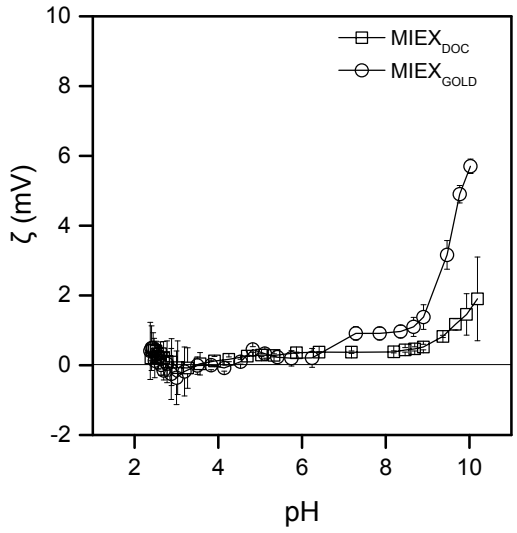

Figure S13. Zeta potential of $MIEX_{DOC}$ and $MIEX_{GOLD}$ in 1 mM KCl electrolyte solution

2. Adsorption kinetic of HA by MIEX at different water chemistry: ionic strength, calcium, pH and HA concentration

HA adsorption kinetics by $MIEX_{DOC}$ was determined at different concentrations of NaCl (range 0-50 mM) and calcium (0-4 mM), at different pH (range 2-10) and HA concentration (4-45 mgC/L)

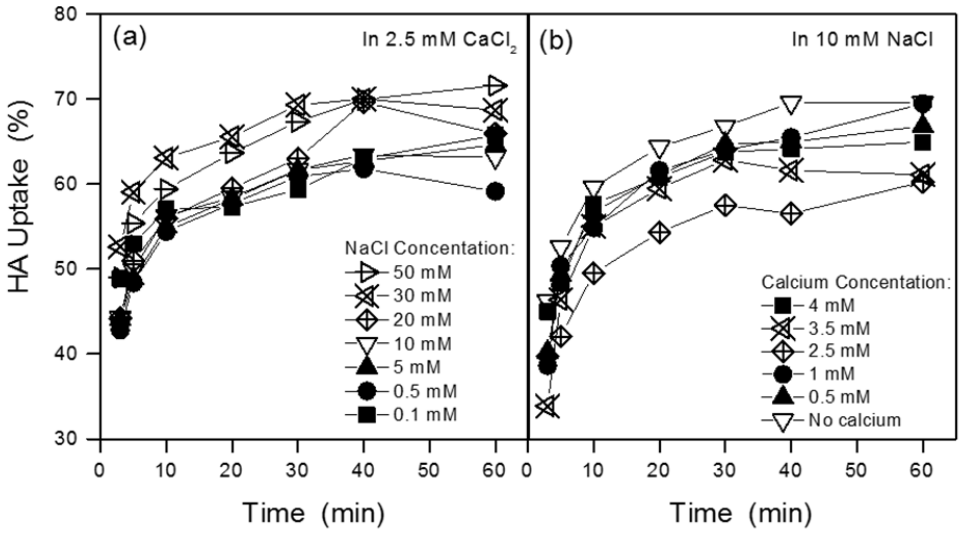

Figure S14. HA uptake kinetics. Influence of (a) Ionic strength (NaCl concentration) and (b) Calcium concentration (12.5 mg/L HA, 1 mM $NaHCO_3$, 10 mL/L MIEX, 20 °C, 260 rpm, pH 6)

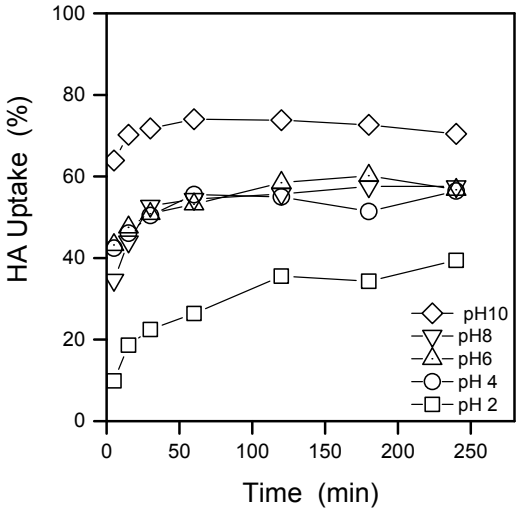

825

826 **Figure S15.** HA uptake as a function of time at different pH (12.5 mgC/L HA, 2.5 mM $CaCl_2$, 1 mM
827 $NaHCO_3$, 10 mM NaCl, 10 mL/LMIEX, 20 °C, 260 rpm)
828

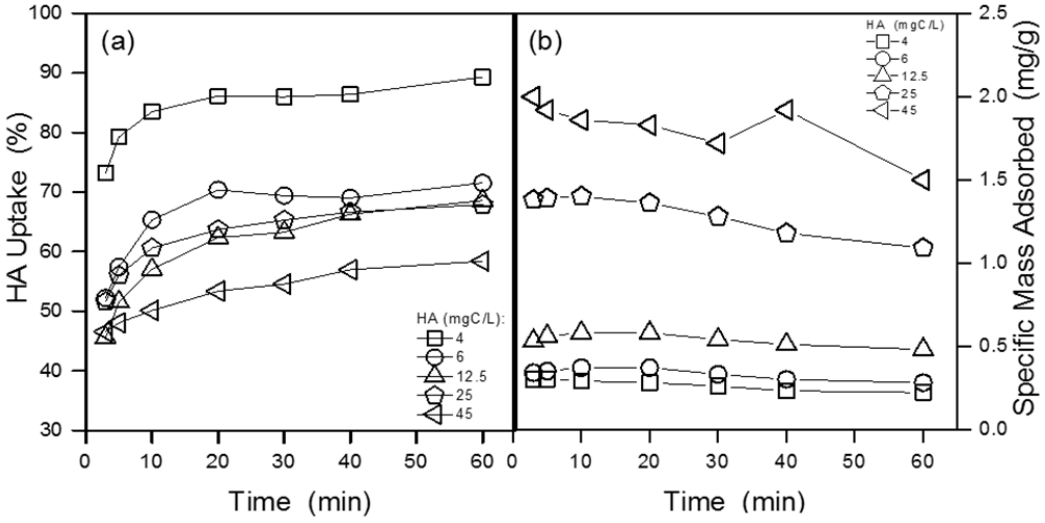

Figure S16. a) HA uptake kinetics at different HA concentrations; b) HA mass adsorbed per unit mass of MIEX as a function of time at different HA concentrations (2.5 mM $CaCl_2$, 1 mM $NaHCO_3$, 10 mM NaCl, 10 mL/L resin, 20 °C, 260 rpm, pH 6)

3. Retention of HA in NF and combined NF-MIEX process

829 Retention of HA as a function of recovery was measured in both NF and NF-MIEX processes.

830 Figure **S17** presents HA retention for both membranes (NF90 and NF270) and both processes (NF and
831 combined NF-MIEX).

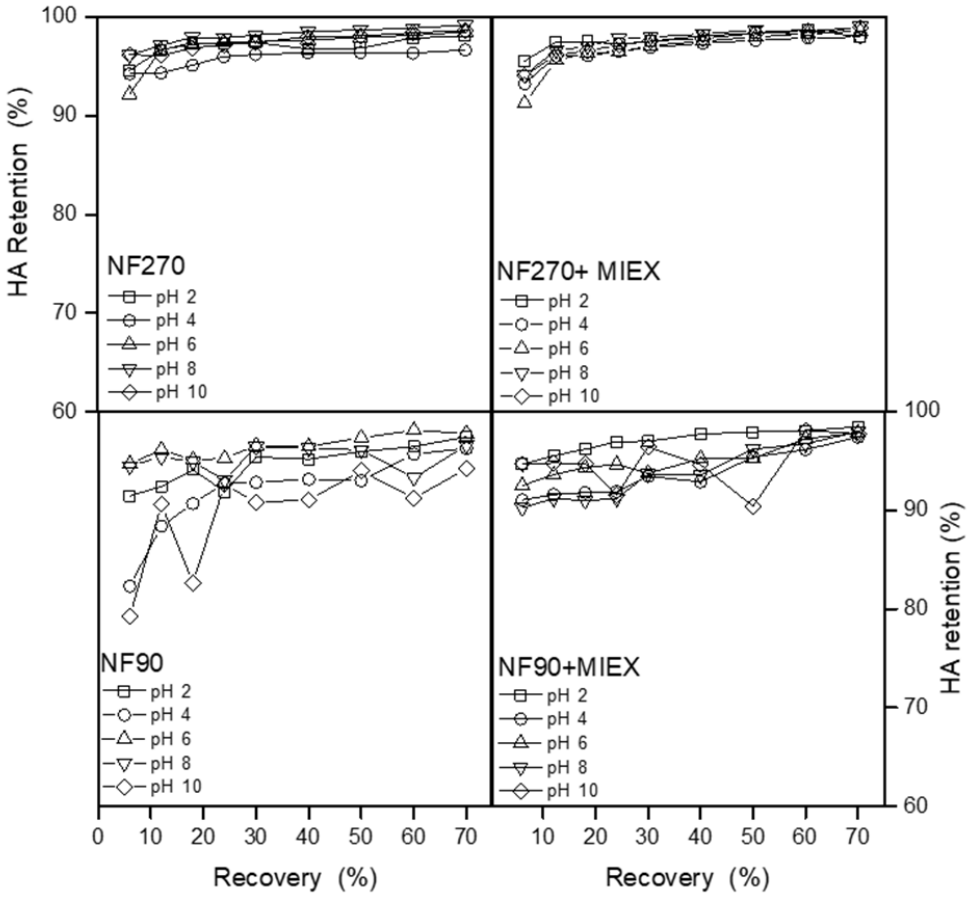

Figure S17. HA retention as a function of recovery at different pH (12.5 mg/L HA, 2.5 mM $CaCl_2$, 1 mM $NaHCO_3$, 10 mM NaCl, 10 mL/L MIEX, 9.6 bar, 400 rpm, 22 °C, 70% recovery)

4. Comparison of normalized permeate flux versus pure water flux (J_{w0}) and initial filtration flux (J_{t0})

Flux decline as a function of filtered volume was calculated by normalizing the permeate flux (J_t) versus J_{t0} (initial filtration flux) or J_{w0} (pure water flux) in order to evaluate comparability and limitations of both methods and the influence of the osmotic pressure. Flux decline in NF and combined MIEX-NF for both NF270 and NF90 membrane samples and at different pH values is reported in Figure S18.When J_{t0} was used to normalize the flux the effect of osmotic pressure was excluded and flux decline started from 1 for each experiment. However, as mentioned in the Material and Methods section, in dead-end system initial unstable conditions occurred due to system adjustment, which introduces limitation to determine precisely J_{t0}. This was visible in the initial part of the graph where an increase in normalized flux was determined due to pressure adjustment. In order to establish a J_{t0} value for each experiment, the flux measured at corresponding pressure of 9.6 bar and stable conditions was considered. The overall trend of flux decline at different pH in both individual NF and combined NF-MIEX process was comparable with the flux decline calculated by using J_{w0} as reference value. In individual NF process, higher flux decline was visible at alkaline pH compared with acidic pH and flux decline was more significant for NF90 compared

with NF270. In combined MIEX-NF process, flux decline was reduced significantly for NF90, while it was negligible for NF270.

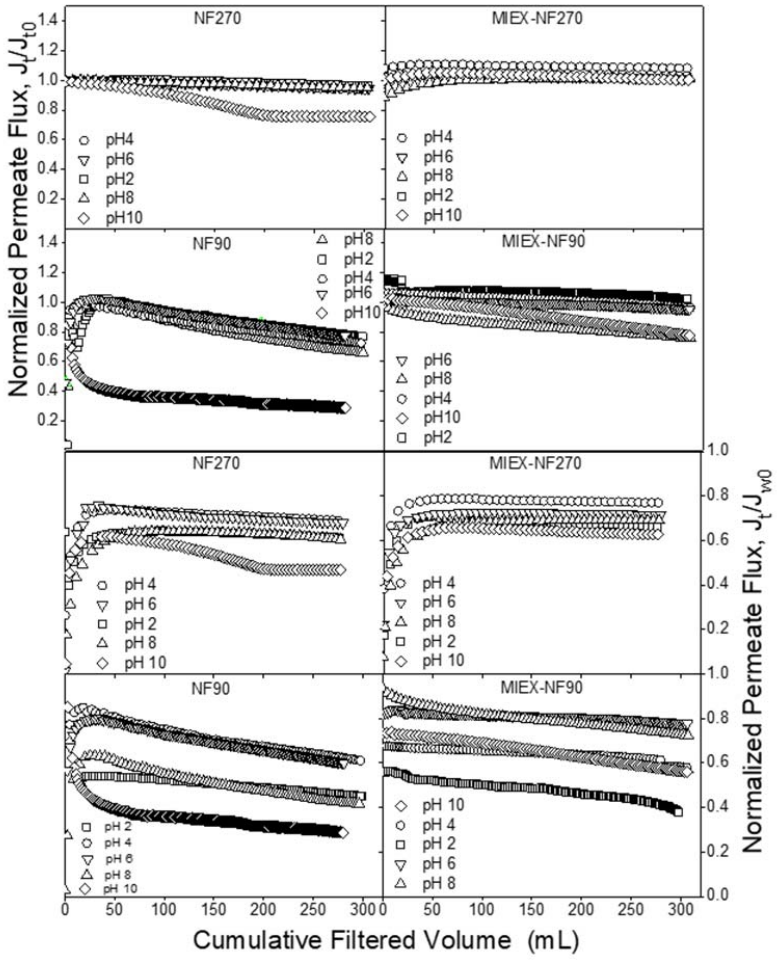

Figure S18. Normalized flux versus J_{t0} (initial flux of fouling experiments) or J_{w0} (pure water flux) as a function of filtered volume

When J_{w0} was used to normalize the flux, the osmotic pressure of the feed solutions was not take into account. As a consequence, the beginning of the flux decline started in a range of 0.8 and 0.6 rather than 1. An osmotic pressure of 0.7 bar is calculated using Van't Off equation by taking into account the concentration of salts in the feed solution (1 mM $NaHCO_3$, 10 mM NaCl and 2.5 mM $CaCl_2$). However, the variation of pH, which caused variation of feed solution ionic strength, is not taken into account in the Van't Off equation. Therefore, conductivity of feed solution at different pH is measured and total dissolved solids (TDS, mg/L) is calculated from the conductivity (EC, µS/cm) by using the equation TDS (mg/L) = EC (µS/cm) · 0.5 [82]. The osmotic pressure (Π, bar) of the feed solution at different pH was estimated by the total dissolved solids (TDS, mg/L) using Equation S1 [83]:

$$\Pi = \frac{(70.7 \cdot TDS \cdot 10^{-6}) + 0.1}{10^{-1}} \qquad \text{Eq (S1)}$$

Variation of osmotic pressure and conductivity of feed solution as a function of pH is reported in Figure S19. In the range of pH 4 to 10 conductivity and osmotic pressure were almost constant at values about 2000 µS/cm and 2 bar, respectively. At extreme pH values (e.g., pH 2 and 12) conductivity increased significantly and as consequence osmotic pressure of about 4.5 bar was estimated, that is about 2 times higher compared with the osmotic pressure calculated for the other pH. This variation of osmotic pressure in addition to permeability variability can be correlated with the variability of the initial trend of flux decline obtained when J_{w0} was used.

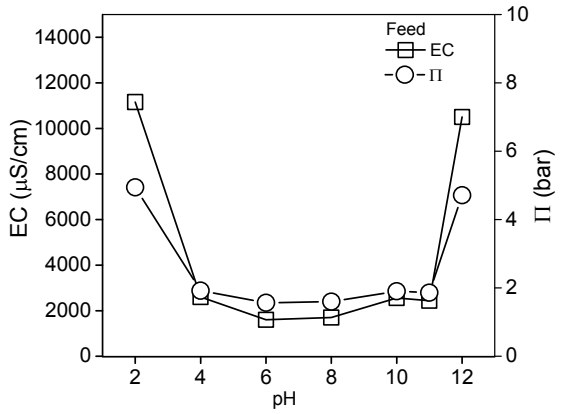

Figure S19. Conductivity and osmotic pressure of feed solution as a function of pH. Osmotic pressure is calculated by using Eq. S1

5. Concentration of inorganic carbon (IC) in the feed, concentrate and permeate

IC and calcium concentration were measured in the feed, concentrate, and permeate samples collected during filtration by NF90 or NF270 for both NF and combined NF-MIEX. The concentration as a function of pH is reported in Figure S20. Calcium concentration in retentate samples is reported both as values measured following filtration (points in bracket) and as values calculated based on mass balance from observed values of feed and permeate samples (using Equation 5 reported in the manuscript). For NF270, measured and calculated concentrations are in accordance, while a discrepancy was observed for NF90.

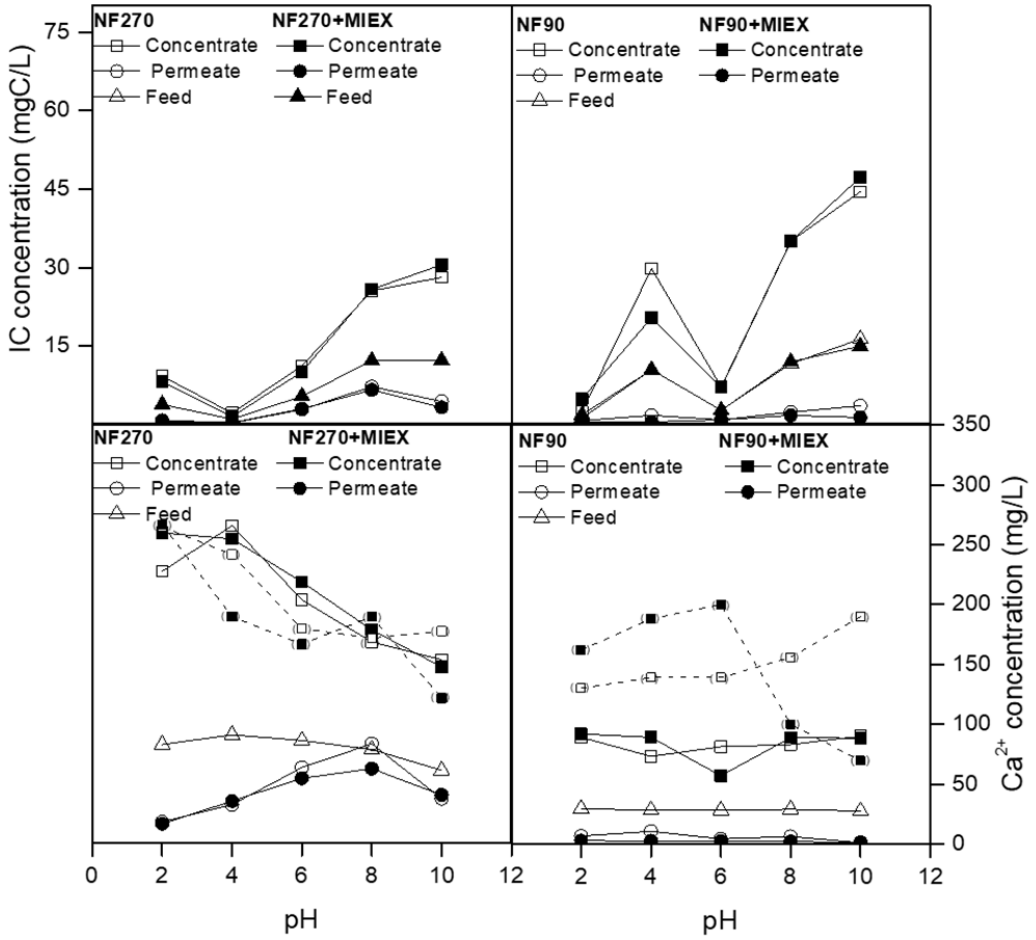

Figure S20. IC and Ca^{2+} concentration in the feed, permeate, and concentrate as a function of pH (12.5 mg/L HA, 2.5 mM $CaCl_2$, 1 mM $NaHCO_3$, 10 mM NaCl, 10 mL/L MIEX, 9.6 bar, 400 rpm, 22 °C, 70% recovery)

6. Error calculation

The system error (ΔS) is calculated from the uncertainties of the various experimental parameters:

$$\Delta S = \sqrt{\Delta T^2 + \Delta V^2 + \Delta P^2}$$

where ΔT is the relative error due to temperature variation, ΔV is the relative error due to volume variation, ΔP is the relative error due to pressure variation.

The flux error (ΔJ) is estimated considering the system error and the variability of pure water flux (ΔJ_{w0})for each membrane sample:

$$\Delta J = J\sqrt{{\Delta J_{w0}}^2 + \Delta S^2}$$

where J is the flux for each experiment. Error for HA uptake (ΔHA) by MIEX is estimated from the uncertainties of the TOC analyzer (ΔTOC).

$$\Delta HA = \sqrt{\Delta TOC^2 + \Delta TOC^2}$$

ΔTOC is considered twice because concentration is considered twice in the calculation of HA uptake.
Error for IC retention (ΔIC) is estimated using the same method published in Supporting Information of another study which takes into account also degassing of carbonate system at acidic pH [63].
Error for Ca^{2+} retention (ΔCa) is calculated from the uncertainties of the ICP-OES (ΔICP).

$$\Delta Ca = \sqrt{\Delta ICP^2 + \Delta ICP^2}$$

The error terms are reported in the table below:

ΔT (%)	**ΔP (%)**	**ΔV (%)**	**ΔS (%)**	**ΔJ (%)**	**ΔTOC (%)**	**ΔHA (%)**	**ΔCa (%)**
5.1	1.4	1.2	20.5	19.8	13.0	18.4	5.7